Epitope Engineered Human Haematopoietic Stem Cells are Shielded from CD123-targeted Immunotherapy

Romina Marone*1,2, Emmanuelle Landmann*1,2, Anna Devaux*1,2, Rosalba Lepore*1,2,3,4, Denis Seyres 1,2, Jessica Zuin 1,2, Thomas Burgold 1,2, Corinne Engdahl 1,2, Giuseppina Capoferri 1,2, Alessandro Dell'Aglio 1,2, Clément Larrue 5,6, Federico Simonetta, 7,8, Julia Rositzka 9,10, Manuel Rhiel, 9,10, Geoffroy Andrieux 11, Danielle Gallagher 12, Markus Schröder 12, Amélie Wiederkehr 4, Alessandro Sinopoli 4, Valentin Do Sacramento 3, Anna Haydn 4, Laura Garcia-Prat 3, Christopher Divsalar 4, Anna Camus 3, Liwen Xu 13, Lorenza Bordoli 14,15, Torsten Schwede 14,15, Matthew Porteus 13, Jérôme Tamburini Bonnefoy 8, Jacob E. Corn 12, Toni Cathomen 9,10, Tatjana I. Cornu 9,10, Stefanie Urlinger 3,4 and Lukas T. Jeker 1,2

* These authors contributed equally

1) Department of Biomedicine, Basel University Hospital and University of Basel, Basel, Switzerland
2) Transplantation Immunology & Nephrology, Basel University Hospital, Basel, Switzerland
3) Cimeio Therapeutics AG, Basel, Switzerland
4) Ridgeline Discovery GmbH, Basel, Switzerland
5) Past: Translational Research Centre in Onco-hematology, Faculty of Medicine, University of Geneva, and Swiss Cancer Center Leman, Geneva, Switzerland
6) Current: Centre de Recherches en Cancérologie de Toulouse, Université de Toulouse, Inserm, CNRS, Toulouse, France

7) Division of Hematology, Department of Oncology, Geneva University Hospitals, Geneva, Switzerland
8) Translational Research Center for Onco-hematology, Department of Medicine, Faculty of Medicine, University of Geneva, Geneva, Switzerland
9) Institute for Transfusion Medicine & Gene Therapy, Medical Center, University of Freiburg, Freiburg, Germany
10) Center for Chronic Immunodeficiency (CCI), Faculty of Medicine, University of Freiburg, Freiburg, Germany
11) Institute of Medical Bioinformatics and Systems Medicine, Medical Center-University of Freiburg, Freiburg, Germany
12) Institute of Molecular Health Sciences, Department of Biology, ETH Zürich, Zürich, Switzerland
13) Department of Pediatrics, Stanford University, School of Medicine, Stanford CA, USA
14) Biozentrum, University of Basel, Spitalstrasse 41, Basel, Switzerland
15) SIB Swiss Institute of Bioinformatics, Spitalstrasse 41, Basel, Switzerland

Author Correspondence:

Lukas T. Jeker, MD, PhD
Department of Biomedicine, Basel University Hospital and University of Basel, Hebelstrasse 20, CH-4031 Basel, Switzerland
E-mail: lukas.jeker@unibas.ch
+41 61 328 50 27

46 **Keywords**

47 Haematopoietic stem cell transplantation (HSCT); targeted immunotherapy; CD123,
48 genome engineering; CRISPR/Cas9; acute myeloid malignancy (AML); molecular
49 shield; epitope engineering; CAR T

Summary

Targeted eradication of transformed or otherwise dysregulated cells using monoclonal antibodies (mAb), antibody-drug conjugates (ADC), T cell engagers (TCE) or chimeric antigen receptor (CAR) cells is very effective for haematologic diseases. Unlike the breakthrough progress achieved for B cell malignancies, there is a pressing need to find suitable antigens for immunotherapy of myeloid malignancies. CD123, the interleukin-3 (IL-3) receptor alpha-chain, is highly expressed in various haematological malignancies, including acute myeloid leukaemia (AML) and blastic plasmacytoid dendritic cell neoplasm (BPDCN). However, shared expression of CD123 on healthy haematopoietic stem and progenitor cells (HSPCs) bears the risk for extensive myelotoxicity upon targeted depletion. Here, we demonstrate that rationally designed, epitope-engineered HSPCs were completely shielded from CD123-targeted immunotherapy but remained fully functional while CD123-deficient HSPCs displayed a competitive disadvantage. Thus, molecularly shielded HSPCs could allow tumor-selective targeted immunotherapy and in parallel enable rebuilding a fully functional haematopoietic system. We envision that this approach is broadly applicable to many targets and cells, could render hitherto undruggable targets accessible to immunotherapy and will allow continued posttransplant immunotherapy, for instance to treat minimal residual disease (MRD) or be used as a salvage therapy. Since the function of the engineered targets is preserved, multiplexed molecular shielding could also enable targeted combination immunotherapies to address tumor heterogeneity. More generally, epitope shielding will be applicable for replacement of other cell types including the many immune cells which are currently being considered for engineered cellular therapies.

73 **Introduction**

74 Targeted cell depletion represents a medical standard of care for several liquid
75 malignancies, autoimmune diseases and prevention or treatment of acute rejection in organ
76 transplantation. Depleting antibodies are mostly IgG but other highly effective targeted
77 immunotherapies work through different mode of action (MoA) and include various
78 antibody-derived molecular formats such as antibody-drug conjugates (ADC),
79 radioimmunoconjugates, T cell engagers (TCE) or chimeric antigen receptor (CAR)
80 bearing cells[1-3]. In the past decade the latter have emerged as a highly effective,
81 programmable cell depletion modality with very high response rates in B cell malignancies
82 and more recently systemic lupus erythematodes[4-9]. The persistence of CD19 CAR T cells
83 can be reliably measured by assessing the duration of B cell aplasia after infusion [5,10,11]. In
84 children and young adults with B-ALL it appears that persistence of CAR T cells is an
85 important requirement for cure[12]. Hence, various strategies to increase CAR T longevity
86 are explored[13,14]. Although high depletion efficiencies can lead to long-term remission,
87 they are associated with the risk for prolonged B cell aplasia due to indiscriminate killing
88 of both normal and tumor B cells, respectively[9,15]. In fact, CAR T cells can persist for a
89 decade and result in years-long B cell aplasia[16]. Such deep purging of a cell type is only
90 acceptable if the depleted cell is dispensable and/or its function can be replaced. Thus, a
91 key to the CAR T field's success was the availability of B cell-restricted target antigens
92 (e.g. CD19) and the possibility to mitigate the loss of co-targeted healthy B cells through
93 infusions of immunoglobulins (IVIG). Given the clinical benefit and the commercial
94 availability of CAR T cells as well as other effective cell depleting modalities, the number

95 of patients at risk for iatrogenic long-term immunodeficiencies through highly efficacious
96 cell depleting therapies are expected to continue to increase rapidly.
97 Unlike the breakthrough progress achieved for B cell malignancies there is a pressing need
98 to find suitable antigens for immunotherapy of myeloid malignancies and particularly acute
99 myeloid leukaemia (AML)[17]. Targeting myeloid malignancies is especially challenging
100 however, since AML displays high clonal heterogeneity, being composed of cells with
101 highly variable surface protein expression[12,17-19]. Importantly, leukaemia stem cells (LSCs)
102 which are phenotypically very similar to HSCs are important targets in (AML)[20].
103 Therefore, most AML candidate targets are co-expressed by HSPCs[17,18]. As a consequence,
104 the risk of myelosuppression associated with myeloid-cell targeted CAR T therapy likely
105 limited the number of clinical trials for AML compared to B cell targeted CAR T trials[12,21].
106 Despite major efforts, single targets with an expression profile as favourable as CD19 could
107 not be identified in AML[17]. Therefore, the paucity or mere absence of cancer-restricted
108 surface proteins constitutes a critical barrier to antigen-specific immunotherapy[11,12,22].
109 A number of solutions have been proposed to overcome the limitations of shared target
110 antigens that underly on-target off-tumour toxicity. Affinity tuning, i.e. reducing a CAR's
111 affinity, can increase the selectivity towards cells with a high antigen expression[23];
112 transient CAR expression (delivery as mRNA) temporally limits CAR activity; and CAR
113 T therapies targeting essential cells, particularly HSPCs, could be used as a bridge to
114 transplant[21,24,25]. However, sparing cells with low antigen expression creates a risk for
115 antigen$^{-/lo}$ relapse[12,26] and the need to remove an effective CAR T therapy targeting HSPCs
116 is neither economically nor scientifically appealing. Therefore, three groups proposed a
117 radical solution: removing the target antigen partially or entirely in HSPCs before

118 haematopoietic stem cell transplantation (HSCT) prevents binding of the immunotherapy
119 to the HSPCs and their progeny and thus creates a synthetic tumor-selectivity[27-29].
120 Preclinical studies demonstrate the feasibility for CD33 and early results from a clinical
121 trial showed a favourable safety profile with engraftment of CD33-deficient $CD34^+$ HSPCs
122 (clinicaltrial.gov NCT04849910)[27-29]. Additional data will be required for further
123 development of this approach. However, the number of truly dispensable antigens is likely
124 limited yet mostly unknown. Moreover, targeting dispensable proteins may favour antigen
125 negative cancer relapses, a phenomenon known to limit long-term outcome of CAR T
126 therapies[26]. Therefore, deliberately targeting essential proteins would be preferrable to
127 reduce the risk for antigen escape. However, this is impossible with a knock-out (KO)
128 approach.
129 Here, we aimed to provide proof-of-concept by engineering HSPCs expressing an
130 endogenous protein variant that completely shields the cells from targeted immunotherapy
131 while preserving its function. The interleukin-3 receptor α chain (IL3RA; CD123)
132 regulates proliferation and differentiation of HSPCs[30], is often expressed on AML LSCs
133 and blasts from relapses[31] and hence is associated with a poor outcome of the disease.
134 Therefore, CD123 constitutes a promising target for AML[19,21] for which multiple
135 therapeutics are being explored preclinically and clinically including IL-3 bound to
136 diphtheria toxin[32], monoclonal antibodies (mAb) blocking IL-3 [33] or engineered for
137 enhanced antibody dependent cellular cytotoxicity (ADCC)[34], an antibody drug conjugate
138 (ADC)[35] and bispecific TCEs, e.g. a CSL362/OKT3-TCE[36,37]. Despite the promising on
139 target toxicity, many of these therapies displayed cytotoxicity towards HSPCs, monocytes,
140 basophils and plasmacytoid dendritic cells (pDCs)[19,21,36]. Thus, protecting HSPCs from the

141 immunotherapies is desirable but due to CD123's role in HSPC biology it is unknown
142 whether a CD123 KO approach would be viable or if a KO approach may result in impaired
143 immune function. We identified multiple single amino acid (aa) substitutions that shielded
144 from ADCC, ADC, TCE and CAR T cell killing while preserving CD123 function. These
145 variants enabled selective TCE- or CAR T-mediated tumour killing while engineered
146 HSPCs were unaffected. CD123 KO HSPCs had a major competitive disadvantage in vitro
147 while engineered CD123 knock-in cells were comparable to wt. Given the favourable
148 safety data, we envision that this approach is broadly applicable, could render undruggable
149 targets accessible to immunotherapy and will allow continued, posttransplant
150 immunotherapy for instance to treat minimal residual disease (MRD) or be used as a
151 salvage therapy.

152 **Results**

153 *Figure 1: Rational design of human CD123 protein variants to shield from targeted*
154 *immunotherapy*
155 CD123 variants were designed *in silico*. We aimed to identify protein variants that are
156 structurally and functionally tolerated, i.e., variants that exhibit a similar structure to
157 wildtype (WT) CD123, that preserve the ability to bind IL-3 and elicit IL-3 mediated
158 downstream cell signalling but are otherwise shielded from the CSL362 antibody or a
159 similar antigen binding moiety. To this aim, available experimentally determined three-
160 dimensional structures of CD123 in different states were used to identify the protein
161 regions involved in binding to CSL362 and IL-3. As previously described[38], the CSL362
162 epitope is located at the N-terminal domain (NTD) of CD123 (**Fig. 1a**), where the CSL362
163 fragment antigen binding (Fab) binds both the "open" and "closed" conformations of the
164 NTD. Based on structural analysis, we identified several CD123 residues as part of the
165 antibody-antigen interface and involved in direct intermolecular interactions with the
166 CSL362 complementarity-determining regions (CDRs) in both conformational states: T48,
167 D49, E51, A56, D57, Y58, S59, M60, P61, R84, V85, A86, N87, P89, F90, S91. Most of
168 these amino acid sites show differential exposure to solvent upon binding of the CSL362
169 antibody, with residues E51, S59, P61, and R84 switching from highly exposed to buried
170 (**Fig. 1b**). E51, S59 and R84 were selected as critical sites for the CSL362 binding (**Fig.**
171 **1c**) and most likely safe for mutagenesis. In contrast, P61 is likely relevant for IL-3 binding
172 due to its close interatomic distance to IL-3 residues and therefore was excluded from
173 further analysis. Comprehensive mutagenesis was performed *in silico* and the mutational
174 effect estimated as statistical energy difference (ΔE) (**Fig. 1d**) with particular focus on the

175 three key residues (**Fig. 1e**) and candidate variants selected upon ranking for decreasing
176 ΔE, for a total of 28 variants (**Fig. 1f**).
177

178 *Figure 2: Preserved expression of engineered CD123 variants despite abolished binding*
179 *to the monoclonal antibody MIRG123*
180 We used a CSL362 IgG1 biosimilar (MIRG123) to experimentally validate its binding to
181 the in silico designed CD123 variants. We generated HEK-293 cells stably expressing
182 human wildtype CD123 (HEK-CD123) or individually harbouring each of the 28 selected
183 amino acid substitutions at positions E51, S59 and R84 (**Fig. 1f**). Using flow cytometry we
184 concomitantly quantified MIRG123 binding as well as preserved expression of the variants
185 by staining with the control anti-CD123 mAb clone 6H6, whose binding to CD123 does
186 not interfere with MIRG123 (**Fig. 2a**). The results revealed a drastic reduction of MIRG123
187 binding to most candidate CD123 variants, and abolished binding to almost half (13/28) of
188 them. Based on the dual staining characteristics to mAbs 6H6 and MIRG123 each variant
189 was categorized as either a non-binding (< 1% double staining to 6H6/MIRG123, 13
190 variants, blue), weak (1-20%, 12 variants, orange) or strong (> 20%, 3 variants, red)
191 binding variant (**Fig. 2b**). The latter showed comparable binding to HEK-CD123. Among
192 the weak binding variants, MIRG123 mostly bound the highest CD123 expressing cells.
193 These results demonstrate the feasibility to rationally design single amino acid substitutions
194 that completely disrupt the binding of a candidate antibody while preserving the expression
195 of the engineered protein.
196

197 *Figure 3: Cells expressing engineered CD123 variants are shielded from multiple*
198 *targeted immunotherapy modalities in vitro*
199 Next, we explored whether the non-binding variants were protected from MIRG123-
200 mediated cytotoxicity either in the format of a mAb (ADCC), a bispecific TCE or human
201 CAR T cells (**Fig. 3a**). First, we tested whether the CD123 variants were shielded from
202 MIRG123-triggered ADCC using an FcγRIIIa expressing reporter cell line. Target cell
203 binding of the test antibody leads to activation of a luminescence signal in the reporter cells
204 through Fc-mediated activation of the FcγRIIIa receptor. High luminescence was measured
205 in the presence of unmodified antigen (HEK-CD123) as well as all strong binding variants
206 (**Fig. 3b**). In contrast and consistent with the flow cytometry data (**Fig. 2a-b**) 12/13 non-
207 binding variants did not induce any ADCC signal above background detected in control
208 cells devoid of CD123 (HEK; lower dashed line) with the exception of S59Y which
209 induced minimal activity. Weak binders showed an intermediate ADCC activity. Thus,
210 ADCC signals positively correlated with the flow cytometry data.
211 Encouraged by these results, we investigated whether the non-binding variants would also
212 protect from more potent immunotherapies such as TCEs and CAR T cells which result in
213 cytotoxicity at a lower antigen density than ADCC-inducing mAbs[39]. First, we co-cultured
214 CD123 expressing HEK-293 cells and human T cells with and without the CSL362/OKT3-
215 TCE (TCE)[37]. After 3 days of co-culture, T cells clustered in the presence of HEK-CD123
216 and TCE, whereas clusters were neither seen with the non-binding variant E51K (or any of
217 the other non-binding variants) nor with the target cells devoid of CD123 (HEK) (**Fig. 3c**).
218 In line with these findings, neither HEK cells nor cell lines expressing non-binding CD123
219 variants were subject to TCE-mediated cytotoxicity. In contrast, some weak binding
220 CD123 variants induced limited cytotoxicity while control HEK-CD123 and strong-

221 binding variants were lysed in the presence of the TCE (**Fig. 3d**). Consistent with these
222 results, upregulation of the activation marker CD69 above background was only detected
223 in T cells in co-culture with HEK-CD123 but not with E51K or HEK (**Fig. 3e**) or any of
224 the non-binding CD123 variants (**Fig. 3f, Extended data Fig. 1a**). In contrast, the
225 frequency of $CD69^+$ T cells increased in the presence of some weak binding variants and
226 was comparable between HEK-CD123 and the strong binding variants. Both $CD4^+$ and
227 $CD8^+$ T cells were activated but $CD8^+$ T cells displayed a higher proportion of activated
228 $CD8^+CD69^+$ effector T cells (**Extended data Fig. 1b-c**). Likewise, secreted IFNγ was only
229 detected in the co-culture supernatants from highly activated T cells triggered by strong
230 antigen binding (**Extended data Fig. 1d**).
231 As a third modality of CD123-targeting immunotherapies we investigated CAR T cells.
232 We used non-viral CRISPR/Cas9-mediated homology directed repair (HDR) to integrate a
233 second-generation CSL362-derived CD123-specific CAR (123CAR) into the T cell
234 receptor α constant region (*TRAC*) (**Extended data Fig. 2a**). Up to 9% of all electroporated
235 $CD4^+$ and $CD8^+$ T cells expressed the 123CAR as assessed by GFP (**Extended data Fig.
236 2b-d**). Correct 123CAR integration at the *TRAC* locus was confirmed by Sanger
237 sequencing (**Extended data Fig. 2e**). GFP^+123CAR T cells were purified by flow
238 cytometry, expanded, and subsequently used for in vitro cytotoxicity assays. CAR-less
239 control T cells or 123CAR T cells were co-cultured for 24h with the CD123 variant
240 expressing target cell lines. Within hours, 123CAR T cells clustered around HEK-CD123
241 cells, whereas neither HEK nor E51K triggered 123CAR T clustering (**Fig. 3g**). As
242 observed for ADCC and TCE, 12/13 non-binding CD123 variants were shielded from
243 cytotoxicity (**Fig. 3h**). The only exception was again S59Y which induced cytotoxicity

244 (**Fig. 3h**) and IFNγ secretion (**Extended data Fig. 2i**). In contrast and different to the
245 results observed for ADCC and TCE, both, weak and strong binding variants triggered
246 strong cytotoxicity (**Fig. 3h**) and IFNγ secretion (**Extended data Fig. 2i**). In accordance,
247 neither HEK nor E51K increased the proportion of activated $CD69^+$ 123CAR T cells above
248 background whereas the frequency of $CD69^+$ 123CAR increased in response to unmodified
249 CD123 (**Fig. 3i**). The exceptions were S59F and S59Y which both induced CD69
250 upregulation in $CD4^+$ and $CD8^+$ 123CAR T cells, respectively (**Fig. 3j; Extended data**
251 **Fig. 2f-h**). However, among the non-binders, only S59Y concomitantly induced CD69
252 upregulation, IFNγ secretion and cytotoxicity whereas S59F resulted in isolated CD69
253 upregulation but neither IFNγ secretion nor cytotoxicity. Thus, in contrast to ADCC and
254 TCE where antibody and T cell effector function correlated well with antibody binding as
255 determined by flow cytometry (**Fig. 3b-f, Fig. 2b**), weak binding CD123 variants induced
256 123CAR T responses comparable to strong-binding CD123 variants. These findings
257 suggest that CAR T cells are more potent than ADCC and TCE and even weak residual
258 binding can result in CAR T activation and elimination of target cells. In summary, we
259 demonstrate that a series of single amino acid substitutions in CD123 are sufficient to
260 completely prevent the activity of an ADCC-inducing mAb, a TCE and a CAR T cell. This
261 suggests that such variant proteins - when engineered into the genome of target cells -
262 might provide protection from different targeted immunotherapy.
263

264 *Figure 4: Biophysical characterization of selected CD123 protein variants*
265 To characterize the effect of the introduced point mutations on the protein biophysical
266 properties, the extracellular domains (ECD, amino acids 19-305) of selected CD123

267 variants were synthesized as soluble proteins. Real time interaction with the immobilized
268 CSL362 was measured using Bio-Layer Interferometry (BLI) at increasing concentrations
269 of soluble CD123 ECD variants. Wildtype CD123 associated rapidly to the antibody
270 CSL362 in a dose-dependent manner (**Fig. 4a**). In contrast, no interaction was observed up
271 to 300nM of the soluble analyte CD123 E51T, a variant characterized as a non-binder by
272 flow cytometry (**Fig. 4a, Fig. 2a, b**). Similarly, no association to CSL362 was observed for
273 other non-binding variants, including E51K, S59P, S59E, S59F, S59R and R84E. Residual
274 CSL362 association was detected at different concentrations of the weak-binding variants
275 E51A, E51Q, R84T and R84Q (**Fig. 4b**). Consistent with the shielding assays (**Fig. 3b-j**),
276 S59Y showed similar residual binding as weak-binders. Importantly, the association to the
277 control antibody 6H6 was preserved in all tested variants, except for R84E (**Fig. 4c**). Next,
278 we assessed the functionality of the variants in terms of binding to IL-3, i.e. the physiologic
279 ligand of CD123, to the immobilized CD123 variants. All tested variants bound to
280 increasing concentrations of IL-3, with S59P and R84E displaying a modest reduction in
281 IL-3 binding (**Fig. 4d**). Lastly, protein thermal stability was assessed by differential
282 scanning fluorimetry (DSF) analysis. Most CD123 variants demonstrated a thermostability
283 comparable to CD123 WT with an unfolding temperature (Tm) of 50°C. In contrast, R84E
284 induced a higher fluorescence signal at ambient temperature and featured a lower Tm
285 (43°C) (**Fig. 4e**). Since R84E showed reduced binding to 6H6, IL-3 and a lower thermal
286 stability compared to wildtype, it was excluded from further experiments. In summary, we
287 identified several protein variants harbouring single amino acid substitutions at two
288 different residues (E51T, E51K, S59E, S59R) that entirely abolish binding to MIRG123

289 but preserve protein stability, binding to the control mAb 6H6 and the receptor's natural
290 ligand IL-3.
291

292 *Figure 5: HSPCs expressing CD123 variants E51K and E51T are functional,*
293 *differentiate normally in vitro and display a good safety profile*

294 Since we used a cell-free system to establish that the selected CD123 variants preserved
295 dose-dependent binding of IL-3, we next aimed to investigate the functionality of E51K
296 and E51T in intact cells. We used CRISPR/Cas9-mediated HDR to engineer the variants
297 into the human erythroleukemia cell line TF-1 whose proliferation and survival is IL-3- or
298 GM-CSF-dependent[40] (**Extended data Fig. 3a**). The genetically engineered cells were
299 cultured with increasing concentrations of IL-3. WT TF-1 displayed IL-3-dependent
300 growth and the two KI populations E51K and E51T demonstrated near overlapping growth
301 curves indicating intact IL-3 sensing and signalling. In contrast, KO sorted cells
302 proliferated considerably less (**Extended data Fig. 3b**). To test the blocking effect of
303 MIRG123, we cultured the cells with a fixed IL-3 concentration but increasing amounts of
304 MIRG123. As reported in a comparable system using BaF3 cells[38], WT cells showed a
305 dose-dependent growth inhibition and died in the presence of antibody concentrations ≥
306 0.036nM. In contrast, E51K and E51T KI cells proliferated irrespective of the MIRG123
307 concentration. KO cells were not affected by MIRG123 but displayed decreased survival
308 compared to WT, E51K or E51T (**Extended data Fig. 3c**).

309 Next, we aimed to engineer clinically relevant HSPCs that can potentially be used to
310 provide a patient with a CD123 immunotherapy-resistant haematopoietic system. We used
311 reagents close to GMP-grade with the goal to provide scientific proof of concept with the
312 potential for clinical translation. To this end, we engineered the variants E51K and E51T

313 into mobilized, $CD34^+$ enriched peripheral blood HSPCs from healthy donors. $CD34^+$
314 HSPCs were electroporated with high fidelity SpCas9 RNPs and single strand
315 oligodeoxynucleotides (ssODNs). CD123 expression was monitored using flow cytometry
316 with the mAbs MIRG123 and 6H6, two and five days post electroporation, respectively
317 (**Fig. 5a, Extended data Fig. 3d**). Preliminary experiments demonstrated that the ssODNs
318 reduced HSPC viability and consequently in vivo engraftment when E51K and E51T
319 HSPCs were compared to HSPCs that were electroporated without a ssODN. Therefore,
320 we designed ssODNs containing the same silent mutations as in the E51K and E51T
321 ssODNs (wt template) and ssODNs containing stop codons in all 3 reading frames (KO
322 template) in order to have similar ssODNs in the control samples. These groups were
323 compared to E51K and E51T KI HSPCs as well as EP only and RNP without ssODN (KO).
324 In comparison to electroporated WT cells (EP), cells receiving RNPs without ssODN
325 displayed only a slightly increased fraction of $MIRG123^-6H6^-$ (KO) cells (**Fig. 5a**). In
326 contrast, HSPCs receiving RNP together with the wt template displayed increased CD123
327 KO, an effect that was further enhanced in the KO template group as has been reported
328 before. The E51K or E51T HSPCs displayed a distinctly different FACS profile. Over time
329 a population with retained 6H6 but abolished MIRG123 binding ($MIRG123^-6H6^+$)
330 gradually appeared (average 10% on day 2; average 21% on day 5 across 8 donors),
331 suggesting that these were E51K or E51T KI HSPCs (**Fig. 5a, b**). Importantly,
332 $CD34^+CD38^-CD90^+CD45RA^-$ cells (HSCs) displayed similar editing rates as the bulk
333 $CD34^+$ HSPCs suggesting that long-term repopulating HSCs (LT-HSC) and multipotent
334 progenitors MPP1 and MPP2 were edited at similar frequencies (**Fig. 5c, Extended data**
335 **Fig. 3e**). Correct editing of E51 (GAG) to K (AAG) or T (ACC) was confirmed by next

336 generation amplicon sequencing (Amplicon-NGS) (**Fig. 5d**). The number of KI reads
337 correlated well with the FACS analysis (**Fig. 5a, b, d**). To investigate whether the variants
338 E51K and E51T preserved IL-3 signalling we analysed pSTAT5 in KI HSPCs and
339 compared them to HSPCs engineered with wt template or KO template. Among $CD123^+$
340 wildtype cells ($MIRG123^+6H6^+$ "wt", left panel) IL-3 induced a bi-modal pSTAT5 signal
341 in both control HSPCs (wt template) as well as E51K and E51T KI HSPCs (**Fig. 5e,**
342 **histograms**). Within $MIRG123^-6H6^-$ CD123 KO cells (KO template) pSTAT5 signalling
343 was abolished (**Fig. 5e, histogram**). In contrast, gating on $MIRG123^-6H6^+$ (KI) cells
344 demonstrated that all E51K and E51T KI cells were $pSTAT5^+$. Thus, we leveraged the
345 ability to discern unedited from edited cells by flow cytometry to demonstrate that all
346 phenotypically defined KI cells transmitted the IL-3 signal. To further characterize the
347 functionality of the engineered HSPCs and to determine the functional relevance of a
348 preserved IL-3/CD123 signalling axis, we analysed the HSPC in vitro differentiation
349 potential in a colony forming assay. Compared to HSPCs that were electroporated only
350 (EP), the number of colonies was reduced in all samples electroporated with a ssODN
351 template (**Fig. 5f**). Among the latter, HSPCs electroporated with the KO template formed
352 the lowest number of colonies. In contrast, E51K and E51T HSPCs formed equal (E51K)
353 or slightly increased (E51T) number of colonies when compared to wt template HSPCs.
354 However, the relative distribution of colonies representing different lineages (erythroid (E)
355 and myeloid colonies (M)) was comparable among all genotypes (**Fig. 5f**). These results
356 suggested that CD123-deficient HSPCs could have a competitive disadvantage compared
357 to WT or KI HSPCs. To verify this, we analysed the allele frequency (genotypes) found in
358 individual single cell-derived colonies and categorized the alleles as "wt" (unedited), "KO"

359 (NHEJ), "ki" (identification of knock-in template) (**Fig. 5g**). In colonies derived from "wt
360 template" we found only paired alleles with the ability to express intact CD123, i.e. indels
361 were only found when the other allele was wt or ki, and no KO/KO sequences were
362 identified. In KO template HSPCs only very few colonies harboured a genotype leading to
363 the absence of CD123 (KO/KO, ki/ki or ki/KO), whereas the majority of colonies were
364 unedited or contained at least one wt allele (wt/wt, wt/KO or wt/ki). Similarly, in E51K
365 and E51T HSPCs we did not find any KO/KO colonies. In contrast, ki/ki colonies were
366 found at least with equal frequency when compared to wt/wt. Thus, there was a strong
367 counterselection against CD123-deficient colonies whereas CD123 KI sequences were
368 found at the expected frequencies. Therefore, the defect of CD123-deficient colonies in
369 Fig. 5f is an underestimate and the real competitive disadvantage of CD123 KO HSPCs is
370 much more pronounced. In contrast, CD123 E51K and E51T KI HSPCs are functionally
371 equivalent to wildtype with regards to colony forming and differentiation potential. This
372 was confirmed by a flow cytometry-based in vitro differentiation assay as all tested
373 genotypes displayed an equal differentiation into $CD33^+$ myeloid and GlycophorinA
374 $(GlyA)^+$ erythroid cells (**Fig. 5h**). Of note, also in the presence of CSL362 conjugated to
375 tesirine via an uncleavable linker (CSL362-ADC) HSPCs differentiated normally in
376 myeloid and erythroid lineages. Finally, we evaluated the resistance of myeloid $CD33^+$,
377 $CD14^+$ or $CD15^+$ cells derived from CD123 engineered HSPCs to CSL362-ADC. CD123
378 expressing $6H6^+$ cells were strongly depleted in EP, wt and KO samples (**Fig. 5i**), whereas
379 E51K and E51T edited cells were largely resistant to CSL362-ADC killing.
380 As an orthogonal engineering approach, we used AAV6-mediated HDR. Consistent with
381 the data from the non-virally engineered HSPCs, IL-3 induced a strong pSTAT5 signal in

382 both control HSPCs (non-edited and CCR5 edited) as well as E51K and E51T KI HSPCs
383 (**Extended Fig. 3f, related to Fig. 5e**). In contrast, CD123 KO cells displayed strongly
384 reduced pSTAT5 signalling. As with the non-virally engineered HSPCs, the relative
385 distribution of colonies representing different lineages (BFU-E & CFU-E, CFU-G/GM and
386 CFU-GEMM) was comparable among all genotypes independent of IL-3 (**Extended Fig.
387 3g, related to Fig. 5h**. Thus, E51K and E51T variants were efficiently engineered into
388 HSPCs using two orthogonal approaches, resulted in functional CD123 receptor expression
389 with intact IL-3 signalling and normal in vitro differentiation capacity yet were shielded
390 from a CD123-targeted ADC.
391
392 To assess the safety of the gRNA used to engineer the E51K and E51T variants we used
393 computational prediction, Discover-Seq[41] and CAST-Seq[42,43]. We used Cas-OFFinder to
394 identify potential off-target sites linked to NGG PAM sequences[44]. Considering sites with
395 a maximum of three mismatches or two mismatches with one DNA and/or RNA bulge
396 identified six candidate off-target sites (OT1-6) (**Fig. 5j and Extended data table 1**).
397 Using these parameters, the gRNA targeting VEGFA resulted in a high number of
398 predicted off-targets as previously reported (high benchmark)[45]. In contrast and in line with
399 previous reports, the gRNA targeting the HBB locus had a low number of predicted off-
400 targets (low benchmark)[41,46]. Compared to these benchmarking gRNAs, the gRNA
401 targeting CD123 had very low numbers of predicted off-targets. Next, we performed
402 Discover-Seq and obtained a typical on-target profile at a good sequencing depth resulting
403 in a Disco score of 207. In contrast, all nominated off-target hits had a very low Disco score
404 (≤9) and at least 5 mismatches. Since Disco scores highly correlate with eventual indel

405 frequencies[41], these results suggested that the nominated off-target hits were likely false
406 positives (**Fig. 5k and Extended data table 2)**. We selected the top 11 nominations for
407 validation by rhAmpSeq and classified all other hits as false positives. Multiplexed
408 amplicon-NGS on the selected 18 loci (1 on target (OnT), 6 computational, 11 Discover-
409 Seq) performed on unedited HSPC and EP ("unedited") and KO template, KO RNP, E51K
410 and E51T samples ("edited") from 4 different donors did not show any evidence of indels
411 (**Fig. 5l**). Finally, as an additional orthogonal assay we performed CAST-Seq analysis,
412 which identifies chromosomal translocations and on-target site aberrations, and nominates
413 off-target sites. An aliquot of the same samples used for Discover-Seq was kept in culture
414 for 5 days post electroporation. In samples edited with RNP complexes, CAST-Seq
415 revealed chromosomal aberrations at the on-target site, such as large deletions and
416 inversions, whereas unedited samples only showcased background activity (**Fig. 5m, left**
417 **panel**). At the same time, off-target mediated translocations could not be detected (**Fig.**
418 **5m, right panel**), confirming the high specificity of the used CRISPR-Cas nucleases. Thus,
419 the selected gRNA did not result in any detectable off-target activity in all the assays
420 performed, demonstrating safe engineering of HSPCs.
421

422 **Figure 6: CD123 epitope engineered HSPCs engraft, differentiate normally and**
423 **possess longterm reconstitution potential in vivo**

424 Next, we tested in vivo engraftment and differentiation potential. We injected the non-
425 virally engineered HSPCs (EP, wt template, KO template, E51K and E51T) into
426 immunodeficient NBSGW mice. After 16 weeks, all mice of the different groups showed
427 comparable engraftment of $hCD45^+$ cells in bone marrow (**Fig. 6a)** and peripheral blood

428 **(Extended data Fig. 4a**). This was also reflected by a comparable frequency and number
429 of human HSCs in the bone marrow (**Fig. 6b**). Furthermore, all groups displayed multi-
430 lineage differentiation in spleen (**Fig. 6c**). Next, we analysed the presence of KI cells
431 among haematopoietic cells in bone marrow. hCD45^{+} cells expressing wt CD123 cells
432 were found with comparable frequencies in all groups. In contrast, E51K and E51T were
433 only found in mice that received KI HSPCs (**Fig. 6d**). We then used the ability to
434 discriminate KI cells from unedited cells to analyse cells with strong CD123 expression.
435 Therefore, we analysed CD123 on pDCs in spleen (gating strategy **Extended data Fig.**
436 **4b**). Although pDC numbers were low, the typical MIRG123^{-}6H6^{+} KI cells were only
437 present in the mice injected with E51K or E51T HSPCs (**Fig. 6e, f**). Thus, engineered
438 HSPCs harbouring single amino acid substitutions engrafted in vivo and differentiated into
439 multiple cell types including pDCs.
440 To investigate whether LT-HSCs were correctly edited and functional we performed
441 secondary transplants. Secondary host mice (NSG-SGM3) transplanted with BM cells
442 from any of the 5 groups demonstrated comparable engraftment (**Fig. 6g**) and frequency
443 and numbers of LT-HSCs in bone marrow (**Fig. 6h**). Furthermore, E51K and E51T
444 engineered HSPCs gave rise to multilineage differentiation comparable to the wt template
445 control mice in spleen (**Fig. 6i**). Importantly, MIRG123^{-}6H6^{+} KI cells were detectable in
446 mice reconstituted with E51K and E51T HSPCs, respectively but not from any of the
447 control HSPCs (**Fig. 6j**). Thus, these data demonstrate that E51K and E51T were
448 engineered into LT-HSCs that retained their engraftment potential and KI cells persisted
449 longterm.
450

451 *Figure 7: Engineered HSPCs enable tumour-selective CD123 immunotherapy*
452 After establishing efficient engineering, a favourable safety profile and demonstration of
453 preserved function and longterm engraftment potential of E51K and E51T HSPCs, we
454 sought to investigate tumour selective CD123-targeted immunotherapy and resistance of
455 engineered HSPCs. We co-cultured engineered HSPCs with control T cells not expressing
456 a CAR ($CD3^+$ CAR neg) or 123CAR (GFP^+) together with the AML cell line MOLM-14
457 ($mCherry^+$). Tumor cells were cleared in all samples with 123CAR but not CAR negative
458 control T cells (**Fig. 7a**). Quantification of HSPCs based on absolute cell counts revealed
459 that wt template $CD34^+$ HSPCs were depleted in comparison to KO HSPCs and E51K and
460 E51T HSPCs (**Fig. 7b**). Since HSPC KO/KI engineering usually remained < 40% (**Fig. 5a-**
461 **d**), a 2-fold reduction of $CD34^+$ HSPCs would be expected due to killing of unedited,
462 CD123 expressing HSPCs. To verify which cells were specifically eliminated we
463 compared the staining profile of CD123 on the remaining $CD34^+$ HSPCs after co-culture.
464 We stained CD123 using only mAb clone 6H6 to avoid possible epitope masking. HSPCs
465 of all 4 groups incubated with CAR negative control T cells expressed CD123 (**Fig. 7c**). In
466 contrast, 123CAR eliminated CD123 expressing cells in wt template HSPCs and KO
467 template HSPCs but not E51K or E51T HSPCs. Thus, 123CAR preferentially depleted
468 highly CD123 expressing HSPCs. However, quantification showed that wt template
469 HSPCs were also depleted among the $6H6^-$ cells since very few cells remained (**Fig. 7c,**
470 **d**). In contrast, E51K and E51T HSPCs were resistant and continued to express CD123. In
471 a similar experiment we incubated MOLM-14 cells (CTV) with non-engineered HSPCs
472 (EP) and 123CAR cells in which case we observed near complete elimination of all EP
473 control HSPCs while E51K and E51T HSPCs were resistant (**Extended data Fig. 5a, b**).
474 Together, these results suggest 123CAR-mediated bystander killing of HSPCs that express

475 low or no CD123. 123CARs also efficiently depleted other AML cell lines (OCI-AML2,
476 OCI-AML3) as well as patient derived AML cells (PDX) (**Extended data Fig. 5c**). Since
477 PDX cells were efficiently killed by 123CAR, we next mixed PDX (CTV^+) with edited
478 HSPCs and 123CAR. As observed for MOLM-14, 123CARs indiscriminately killed PDX
479 as well as wt template HSPCs (**Fig. 7e, f**). In contrast, 123CAR displayed selective
480 cytotoxicity towards PDX cells but preserved E51K and E51T HSPCs (**Fig. 7e-h**).
481 Next, we investigated selective cancer immunotherapy by the TCE and ADC. The
482 CSL362/OKT3-TCE was less potent than the 123CAR since some MOLM-14 cells
483 remained (**Extended data Fig. 5d**). Nevertheless, we also observed an overall depletion of
484 EP HSPCs suggesting some bystander killing of HSPCs expressing low or no CD123
485 (**Extended data Fig. 5d, e**). To exclude possible artifacts due to epitope masking by
486 remaining CSL362/OKT3-TCE that could block MIRG123 binding, we performed an
487 experiment without MOLM-14 cells and FACS-sorted HSPCs based on 6H6 staining on
488 the day of analysis. Sanger sequencing confirmed that EP HSPCs ($6H6^-$ and $6H6^+$) and
489 $6H6^-$ cells sorted from E51K and E51T HSPCs were primarily WT (**Extended data Fig.
490 5f**). Thus, these are HSPCs that have a CD123 WT genotype but do not express CD123. In
491 contrast, sorted $6H6^+$ KI HSPCs were almost purely E51K (AAG) or E51T (ACC),
492 respectively. Thus, E51K and E51T expressing HSPCs withstood CD123-targeted TCE-
493 mediated cytotoxicity leading to an enrichment of edited KI HSPCs. To test ADC as a
494 depletion modality we tested selective tumour killing with MOLM-14 and engineered
495 HSPCs. The CD123-ADC depleted CD123 expressing $6H6^+$ HSPCs but not E51K or E51T
496 HSPCs (**Extended data Fig. 5h**). Thus, engineered KI HSPCs were also shielded from an
497 ADC. However, MOLM-14 cells were not depleted and HSPC numbers for EP, E51K and

498 E51T remained the same (**Extended data Fig. 5g**). Thus, we did not observe any bystander
499 killing by this CD123-targeted ADC but overall efficacy was limited. In summary, epitope
500 engineered, shielded HSPCs can safely be generated, are functional but resistant to CD123-
501 targeted immunotherapy and thereby enable tumour-selective targeting.

502 **Discussion**

503 HSCT is a potentially curative approach for haematologic diseases. A conditioning phase
504 prepares the transplantation of autologous or allogeneic HSCs which, after engraftment,
505 will rebuild a new haematopoietic and immune system. The conditioning serves to remove
506 host HSCs and can kill tumour cells when HSCT is applied for malignant diseases.
507 However, current untargeted cytotoxic conditioning regimens have been directly or
508 indirectly associated with transplant related morbidity and mortality. With the advent of
509 highly effective targeted depleting agents such as mAbs, ADCs, TCEs and CAR T cells it
510 may become possible to replace untargeted conditioning and tumour control by antigen-
511 specific immunotherapy[25,47-50]. However, the absence of suitable antigens constitutes a
512 major impediment to progress in this field[11,12,22]. In particular, targeting LSCs would be
513 highly desirable to treat AML but the risk for myelosuppression arising from shared antigen
514 expression of LSCs and healthy HSCs precludes a continuous posttransplant therapy[25]. As
515 a compromise, it was proposed to use CAR T cells directed against CD123 or CD117 to
516 purge tumour cells and HSCs alike, followed by myeloablative conditioning to remove the
517 CAR T cells before HSCT[21,24,25]. Recently, CAR T cells targeting CD7 were used clinically
518 to deeply purge relapsed T cell acute lymphoblastic leukaemia[51]. However, the CAR7 were
519 only used for a limited time before HSCT and they led to multilineage cytopenia. Thus, the
520 targeted immunotherapy was limited to the pretransplant period and only served as a
521 bridge-to-transplant. However, the ability to continue immunotherapy posttransplant
522 would be highly desirable to eliminate MRD and prevent relapse longterm.

523 We previously used genome engineering to substitute single amino acids in surface
524 proteins of murine T cells which completely abolished binding of specific mAbs[52]. Since

525 we converted protein variants known to have exchangeable function (aka congenic
526 markers) the results suggested that engineering a minimal alteration in surface proteins
527 could enable safe cell shielding for therapeutic purposes. To enable HSCT with continuous
528 antigen-specific immunotherapy, we engineered human HSPCs to express epitope
529 engineered CD123 and demonstrate that these cells are both shielded and functional,
530 respectively. We used structural information to identify at least one aa substitution that
531 completely abrogated mAb binding for 3 separate residues. This is important since it
532 increases the chances that an appropriate genome engineering strategy can be found to
533 safely and efficiently insert a variant into primary therapeutic cells. The choice of the most
534 suitable genome engineering approach will depend on the desired aa substitution and cell
535 type. To establish feasibility, we employed CRISPR/Cas9-mediated HDR which provides
536 flexibility and precise programmability through a DNA template encoding the desired
537 amino acid exchange. Despite some shortcomings such as cellular toxicity, HDR-mediated
538 HSPC editing is safe and clinically relevant[53,54]. In fact, we did not find any detectable off-
539 target activity using multiple complementary assays, demonstrating safe engineering of
540 HSPCs. However, for clinical translation additional studies will be needed, e.g.
541 tumorigenicity studies. In addition, more recently developed genome engineering
542 approaches provide additional options. Specifically, base editing is well tolerated, can
543 achieve high editing efficiencies in HSPCs and is suitable for multiplexed editing[55].
544 However, base editors have different constraints than HDR since they typically only
545 convert A->G or C->T, also have PAM restrictions and the editing window - despite being
546 limited - can result in unwanted bystander editing. As a consequence, base editing can only
547 install a fraction of desired codon changes for a particular aa change. Indeed, we found that

548 these inherent limitations are relevant when using base editors to install cell shielding
549 variants because the most suitable amino acid substitutions may not be accessible to base
550 editing or bystander editing may affect the function of the engineered protein (Marone &
551 Jeker, unpublished observations). Therefore, careful characterization of the editing
552 outcome and the resulting protein variants is required (Garaudé & Jeker, unpublished
553 observations). Prime editing employs a templated approach that also avoids dsDNA breaks
554 and provides the greatest flexibility to install any desired codon change and could therefore
555 be suitable for epitope engineering[55]. However, prime editing was only recently shown to
556 work in HPSCs and further investigation is needed[56].
557 Information about naturally occurring polymorphisms without known disease association
558 (e.g. CD123 E51K) could inform variant choice from a safety perspective. For instance,
559 although IL-3 binding to CD123 E51K may be slightly reduced compared to WT CD123
560 (**Fig. 4d**), it appears that different binding strengths to IL-3 may be biologically tolerated.
561 Theoretically, allogeneic HSPC donors could be pre-screened for such variants which
562 would provide shielding without the need to engineer the cells. However, practically, most
563 polymorphisms are likely too rare since HSPCs also have to be matched for HLA.
564 Conversely, this indicates that some patients receiving therapeutic cell depleting agents
565 may be non-responders due to genetic variation. Remarkably, our results show that a single
566 aa substitution is sufficient to protect from mAb (ADCC), ADC, TCE and even CAR T
567 cells. Thus, shielded HSPCs or other therapeutic cells could be combined with a broad
568 range of available cell depleting agents. However, our data shows that careful
569 characterization of the variants for potential clinical translation is important. For instance,
570 although R84E shielded from all tested depletion modalities, it showed signs of reduced

571 stability. Furthermore, S59P and R84E both showed reduced IL-3 binding and therefore
572 were not further pursued. In addition, the degree of binding reduction will be relevant for
573 the choice of the MoA of the depleter. For instance, S59Y, R84T and R84Q protected from
574 ADCC and TCE but led to substantial killing by the CAR T cells. It is noteworthy that the
575 CAR T response was rather digital with non-binders being protected whereas weak binders
576 resulted in strong CAR T activation and cytotoxicity. In contrast, responses to weak binders
577 were more analogue for ADCC and TCE resulting in much more limited killing. The
578 sensitivity of CAR T responses even to weak binding will also be important when
579 considering targets with expression by non-hematopoietic cells. For instance, although Flt3
580 could be an attractive target to treat AML, Flt3 inhibitors may lead to acute cardiotoxicity[57].
581 Flt3 expression was found in murine cardiomyocytes and expression in human iPS-derived
582 cardiomyocytes was sufficient to result in mild but detectable activation of Flt3-targeted
583 CAR T cells[58,59]. Thus, the therapeutic window created by a shielding variant will be a
584 function of the binding reduction between the WT and the engineered variant, the
585 expression on the target cells (which may be dynamic), expression on non-hematopoietic
586 cells as well as the efficacy of the depleting agent. In some cases, e.g. when a blocking Ab
587 is used, residual binding of the shielding variant may be acceptable. In others, when the
588 variant is to be paired with a highly effective depleter (e.g. ADC or CAR T), the non-
589 binding must be more stringent.
590 In order to fully exploit the advantage of combining shielded HSPCs with targeted
591 immunotherapy, the function of the antigen should be preserved[11]. Our results show that
592 CD123-deficient HSPCs had a competitive disadvantage in vitro and CD123 KO HSPCs
593 were strongly depleted. In contrast, selected shielded CD123 single amino acid substitution

594 variants preserved IL-3 binding, signalling (p-STAT5) and IL-3 dose-dependent growth.
595 Furthermore, engineered KI HSPCs differentiated normally in vitro, engrafted and
596 displayed multi-lineage differentiation potential in vivo. Secondary transplantation
597 experiments confirmed successful engineering of longterm reconstituting LT-HSCs. Thus,
598 molecularly shielded HSPCs could allow tumour-selective CD123 targeted
599 immunotherapy and in parallel enable rebuilding a CD123 variant-expressing
600 haematopoietic system. For instance, CD123 targeting therapies are clinically successful
601 for the treatment of BPDCN, a pDC-derived neoplasm. However, also healthy pDCs
602 strongly express CD123 and therefore will be depleted by any effective CD123
603 immunotherapy. Yet, pDCs are primary producers of type I interferon and hence anti-viral
604 immunity. Their importance was recently illustrated for the protective immunity against
605 SARS-CoV-2 [60]. Therefore, transplanting CD123-shielded HSPCs may in the future
606 potentially allow to fully restore immunity with a completely functional haematopoietic
607 system while simultaneously allowing efficient tumour immunotherapy. More broadly, we
608 envision that function-preserving but shielding variants could be identified for other
609 proteins that currently cannot safely be targeted. Applications could include T cell
610 malignancies since T cell deficiency results in unacceptably severe immunosuppression
611 and T cell function cannot readily be replaced. CD7 is of interest to treat T cell
612 malignancies and AML but CAR7 are currently only used as a bridge-to-transplant[51].
613 Importantly, preserving the function of the engineered proteins could enable multiplex
614 shielded HSPCs that are resistant to combination immunotherapies to address disease
615 heterogeneity. However, safety of multiplex edited HSPCs would need to be assessed
616 carefully. In addition, directed ablation of HSPCs or more generally haematopoiesis has

617 been a long-standing goal to improve HSCT[11] and could be applied beyond malignancies.
618 CD117 and CD45 are promising targets but current approaches are limited to short-term
619 depletion[24,25,47-50]. Targeting CD45 could be applied to systemic autoimmune diseases but
620 it is currently unknown whether short-term depletion will be sufficient and clinically
621 tolerated[48,61,62]. Shielded CD45 variants could enable a gradual replacement of the
622 haematopoietic system including autoreactive lymphocytes. Finally, epitope shielding
623 could open up development of new immunotherapies against as yet unidentified targets
624 and may be applicable for replacement of other cell types e.g. T, B and the many other
625 immune cells which are currently being considered for engineered cellular therapies[11].

Acknowledgements

We acknowledge the contributions of the following research core facilities at the University of Basel and the Department of Biomedicine: the teams of the animal facility for expert animal husbandry and the flow cytometry core facility for excellent support. We thank Marko Hasiuk for gRNA design; Jonathan Knowles for critical reading of the manuscript; Dario Neri and Mihaela Zavolan for sharing reagents; Marko Hasiuk, Simon Garaudé and Hanna Studer for experimental support; Andreas Zingg for advice for CAR T experiments. Some figures created with BioRender.com. This project has received funding from the European Research Council (ERC) under the European Union's Horizon 2020 research and innovation programme (grant agreement No. 818806 to L.T.J.). J.E.C. and D.G. are supported by the NOMIS Foundation, the Lotte and Adolf Hotz-Sprenger Stiftung, SNSF grant 310030_188858, and the Helen Hay Whitney Foundation. T.Ca. and T.I.C. acknowledge funding from the German Federal Ministry of Education and Research (BMBF) within the Medical Informatics Funding Scheme - EkoEstMed–FKZ 01ZZ2015 (G.A.).

Author contributions

These authors contributed equally: R.M., E.L., A.D., R.L.; E.L., A.D., R.M. designed and performed most experiments, analysed data and wrote the manuscript; R.L. designed and performed computational analysis and wrote the manuscript; C.E., A.W., L.G.P., L.X. performed experiments and analysed data; G.C. performed experiments and produced the TCE; F.S. generated and provided MOLM-14-mCherry-luciferase cells; C.L. and J.T.B.

648 generated and provided AML PDX samples; A.DA. performed in vivo experiments
649 supervised by R.M.; J.Z. and T.B. performed and analysed rhAmpSeq; D.S. analysed NGS
650 data; A.S., A.H., A.C. performed protein stability experiments; V.DS., C.D. performed
651 HSPC isolation; D.G., M.S. performed Discover-Seq and bioinformatics analysis under
652 supervision of J.E.C; J.R., M.R., G.A. performed CAST-Seq and bioinformatics analysis
653 under supervision of T.I.C. and T.CA.; L.B. performed initial computational analysis; T.S.
654 supervised computational analysis; M.P. supervised AAV experiments; S.U. designed and
655 supervised experiments; L.T.J. conceived the study, supervised experiments, acquired
656 funding and wrote the manuscript. All authors read and approved the manuscript.
657

658 **Declaration of interests**

659 Funding: Research was supported by the European Research Council (L.T.J.). Sponsored
660 research agreement with Cimeio Therapeutics AG (Cimeio) (L.T.J., M.P., T.I.C.). Cimeio
661 scientists actively contributed to the research and are therefore listed as co-authors.
662 Decision to publish was the sole responsibility of L.T.J. L.T.J.'s employer, the Basel
663 University Hospital, receives financial compensation for L.T.J.'s consulting. Employment:
664 Ridgeline Discovery GmbH: R.L., A.W., A.S., A.H., C.D., S.U.; Cimeio Therapeutics AG:
665 R.L., V.DS., L.G.P., A.C., S.U.; Personal financial interests: L.T.J.: co-founder, board
666 member of Cimeio; Holding Cimeio equity: University of Basel, R.L., A.W., A.S., V.DS.,
667 A.H., L.G.P., C.D., A.C., S.U., L.T.J.; inventors on a patent application related to the
668 findings reported here: E.L., A.D., R.L., R.M., A.W., A.S., A.H., A.C., S.U., L.T.J.; JEC
669 is a cofounder and SAB member of Spotlight Therapeutics, an SAB member of Hornet
670 Bio, and has consulted for Cimeio Therapeutics. The lab of JEC has funded collaborations

671 with Allogene and Cimeio; T.Ca. is an advisor to Cimeio Therapeutics, Excision
672 BioTherapeutics, GenCC, and Novo Nordisk. T.Ca. and T.I.C. have a sponsored research
673 collaboration with Cellectis. T.Ca. and G.A. hold a patent on CAST-Seq (US11319580B2);
674 F.S. consulting fees from BMS/Celgene, Incyte, Kite/Gilead; speaker fees from
675 Kite/Gilead, Incyte; travel support from Kite/Gilead, Novartis, AstraZeneca, Neovii,
676 Janssen; research funding from Kite/Gilead, Novartis, BMS/Celgene. All other authors do
677 not declare any conflict of interest.
678

679 **Data availability Statement**

680 Datasets are available from the corresponding author on reasonable request.

681 ## Materials and Methods

682 All antibody sequences, gRNAs, oligos and flow cytometry antibodies used in the study
683 are listed in Extended data table 4.

684

685 *Structural dataset and computational design of CD123 protein variants*

686 Experimentally determined three-dimensional structures of the CD123 protein were
687 retrieved from the PDB and include (i) the CD123-CSL362 complex in open and closed
688 conformation (PDB ID: 4JZJ[1]), (ii) the CD123-IL-3 binary complex (PDB ID: 5UV8[2]),
689 (iii) the CD123 unbound structure extracted from the complex in open and closed
690 conformation. Given the structure of the complexes, the CSL362 and IL-3 epitopes were
691 defined as the sets of CD123 residues having at least one atom within 4Å to any CSL362
692 and IL-3 atoms, respectively. Per-residue relative solvent accessibility area was computed
693 using the Lee & Richards algorithm[3] implemented in FreeSASA[4], using default parameters
694 and upon removing crystallographic waters, sugars and ions. Comprehensive mutagenesis
695 was performed *in silico* using the EVmutation sequence-specific probabilistic model[5] and
696 the mutational effect, defined as statistical energy difference ΔE, estimated using the
697 epistatic coevolutionary analysis framework[6s8]. For a given mutant, the ΔE is computed as
698 the sum of differences of the constraints on individual amino acid sites plus the sum of
699 differences of the coupling parameters computed for all pairs of sites involving the mutated
700 site. In order to quantify the total epistatic constraint acting on a given amino acid site of
701 interest, evolutionary coupling analysis was run on a multiple sequence alignment (MSA)
702 spanning the entire CD123 sequence. The MSA was built using five iterations of the
703 jackhammer HMM search algorithm against the non-redundant UniProtKB database[9] and

704 default significance score for inclusion of homologous sequences. As values of ΔE below,
705 equal and above 0 correspond to putatively beneficial, neutral, and deleterious effects,
706 respectively, variants at a given site were selected upon ranking for decreasing ΔE.
707

708 *Eukaryotic cell lines*
709 Freestyle CHO-S cells were purchased from Thermo Scientific (Cat#R80007) and were
710 expanded in PowerCHO 2 Serum-free Medium (Lonza BELN12-771Q) supplemented
711 with GlutaMAX (Gibco), HT supplement (Cat# 41065012) and antibiotic-antimycotic
712 (Cat#15240062), to a maximum density of $20x10^6$ cells/ml. TF-1 were purchased from
713 DSMZ (Cat#ACC334) and maintained in RPMI-1640 media supplemented with 10% heat-
714 inactivated FCS (Gibco Life Technologies), 2mM GlutaMAX and 2ng/ml hGM-CSF (215-
715 GM, Bio-Techne). HEK-293 cells were a kind gift of M. Zavolan (Biozentrum Basel) and
716 cultured in Dulbecco's Modified Eagle's Medium - high glucose (Sigma-Aldrich)
717 supplemented with 10% heat-inactivated FCS and 2mM GlutaMAX. MOLM-14 were
718 purchased from DSMZ (Cat#ACC777) and K562 were purchased from ATCC (Cat#CCL-
719 243). Both cell lines were maintained in RPMI-1640 media supplemented with 10% heat-
720 inactivated FCS (Gibco Life Technologies) and 2mM GlutaMAX. All cell lines were
721 freshly thawed and passaged 3-6 times prior to use. AML cell lines (MOLM-14, OCI-
722 AML-2 and OCI-AML-3) were retrovirally transduced with MI-Luciferase-IRES-mCherry
723 (gift from Xiaoping Sun, Addgene plasmid #75020; http://n2t.net/addgene:75020;
724 RRID:Addgene_75020). Cells were then FACS-sorted based on mCherry expression.
725 After expansion, cells were STR profiled and tested mycoplasma negative before being
726 frozen until further use.
727

728 *Hematopoietic cells from human subjects (PDX)*

729 De-identified patient-derived AML samples were obtained from PDX repository (Cancer
730 Research Center of Toulouse, France)[63,64]. Cells were propagated in NSG mice for 2
731 generations. A signed written informed consent for research use in accordance with the
732 Declaration of Helsinki was obtained from patients.

733

734 *Cloning and expression of recombinant wildtype human CD123 and its variants*
735 Full length cDNA of human CD123 (NM_002183.2) was obtained from a pCMV3 vector
736 (Cat#HG10518-M, Sino Biological). The Hygromycin sequence was replaced by a
737 Neomycin resistance cassette by Gibson Assembly. The point mutations of the human
738 CD123 variants were introduced into the vector using PCR (see Extended data table). $2x10^6$
739 HEK-293 cells were electroporated with the pCMV3 vector encoding CD123 wildtype or
740 its variants using the Neon Transfection System (ThermoFisher; 1100V, 20ms, 2pulses).
741 To generate stable cell lines Geneticin G418 (50mg/ml; BioConcept) was added to the cell
742 culture medium at a concentration of 350µg/ml.

743

744 *Cloning and expression of the monoclonal antibody CSL362 biosimilar (MIRG123)*
745 The heavy and kappa light chain variable regions (VH and VKL) of CSL362 were derived
746 from the CSL362/OKT3-TCE[10]. To generate the monoclonal IgG1 antibody CSL362
747 biosimilar MIRG123 the VH and VKL sequences were cloned into AbVec2.0-IGHG1
748 (Addgene plasmid # 80795) and AbVec1.1-IGKC (Addgene plasmid # 80796),
749 respectively, kindly provided by Hedda Wardemann[11]. $2x10^9$ Freestyle CHO-S cells were
750 resuspended in 500ml ProCHO 4 Protein-free Medium (Lonza, Cat#BEBP12-029;
751 supplemented with 1XHT, GlutaMAX, antibiotic-antimycotic) and co-transfected with

752 both plasmids (0.6mg each) using 5mg polyethyleneimine (PEI, Polysciences, Cat#23966).
753 The cells were expanded under constant rolling (140rpm) at 31°C, 5% CO_2 for 6 days. The
754 Freestyle CHO-S cells were pelleted and the filtered supernatant (0.22µm filter) was
755 applied on a Protein A column for purification. CSL362 biosimilar was eluted with 0.1M
756 glycine (pH=2.2), 0.5ml fractions were collected and OD_{280} was measured using a
757 Nanodrop spectrophotometer. The high-concentration fractions were pooled and dialyzed
758 twice overnight in PBS.

759 *Expression and purification of CSL362/OKT3-TCE*
760 The design of the CSL362/OKT3-TCE was recently described[10] and the plasmid was a
761 kind gift from D. Neri (ETH Zurich). Freestyle CHO-S producer cells were transfected
762 using PEI (as described above) with 1.7mg TCE DNA. Following 6 days of expansion the
763 filtered cell culture supernatant was applied to a 5ml Ni-NTA column (ThermoFisher)
764 prewashed with 100ml washing solution (PBS, 150mM NaCl, 5mM Imidazole, pH7.4) for
765 protein purification. The eluted and dialysed TCE was filtered (0.22µm) and stored in
766 aliquots (1mg/ml) at -80°C.
767

768 *Flow cytometry and cell sorting*
769 Flow cytometry was performed on BD LSRFortessa with the BD FACSDiva Software, and
770 the data was analysed with FlowJo Software. Antibodies used for flow cytometry can be
771 found in the Extended data table. For cell sorting the cells were pelleted and resuspended
772 in FACS Buffer (PBS + 2%FCS) supplemented with 1mM EDTA, and sorting was
773 performed either on BD FACSAria or BD FACSMelody Cell Sorter. The control cells were
774 also subjected to the sorting process.
775

776 *Primary human T cell isolation and culture*
777 Leucocyte Buffy coats from anonymous healthy human donors were purchased from the
778 blood donation centre Basel (Blutspendezentrum SRK beider Basel, BSZ). Peripheral
779 blood mononuclear cells (PBMCs) were isolated by density centrifugation using SepMate
780 tubes (Stemcell technologies) and the density gradient medium Ficoll-Paque (GE
781 Healthcare) according to the manufacturer's protocol. Human T cells were purified (> 96%
782 purity) by magnetic negative selection using an EasySep Human T Cell Isolation Kit
783 (Cat#17951, Stemcell Technologies) according to the manufacturer's instruction. If frozen
784 PBMCs were used, T cells were isolated after thawing and cultured in supplemented media
785 without stimulation overnight. T cells were cultured in RPMI-1640 Medium (Sigma-
786 Aldrich) supplemented with 10% heat-inactivated human serum (AB^+, male; purchased
787 from BSZ Basel), 10mM HEPES (Sigma-Aldrich), 2mM GlutaMAX, 1mM Sodium
788 Pyruvate, 0.05mM 2-Mercaptoethanol, 1% MEM Non-essential amino acids (100x) (all
789 Gibco Life Technologies) and IL-2 150U/ml (Proleukin, University Hospital Basel). The
790 medium and IL-2 was replenished every 2 days, and the cells were kept at a cell density of
791 $1x10^6$ cells/ml.
792

793 *ADCC assay (FcγRIIIa activation assay)*
794 ADCC assay was performed using the ADCC Reporter Bioassays, V Variant (Promega,
795 Cat#G7015) according to the manufacturer's instructions. Target cells HEK-293
796 expressing the CD123 variants were seeded in white 96 well-plate clear bottom at 4400
797 cells/100µl culture medium. At day 1, medium was removed and effector cells
798 (Jurkat/FcγRIIIa/NFAT-Luc cells; E:T ratio 12:1) and MIRG123 antibody (final
799 concentration 1µg/ml) were added and incubated for 5h at 37 °C 5% CO_2. The emitted

800 luminescence was read 10min after the addition of Bio-Glo Luciferase Assay Reagent
801 (Promega) using the PHERAstart FSX (BMG LABTECH) program Luc-Glo (LUM),
802 GainA=3600, Optic module=LUMplus. Raji cells incubated with 1µg/ml of anti-CD20
803 antibody rituximab were used as positive control.

804 *In vitro TCE-mediated killing assay with primary T cells*
805 For the TCE killing assays the HEK-293 target cells were co-cultured together with human
806 effector T cells and the CD3/CSL362-TCE at an effector to target ratio of 10:1 for 72 h.
807 One day prior to co-culture HEK, HEK-CD123 and the HEK expressing the CD123
808 variants were stained with CellTraceViolet (CTV) according to the manufacturer's
809 protocol. The following day effector T cells were added with the TCE at a concentration
810 of 300ng/ml and kept for 72h at 37 °C. Cytotoxic activity and activation of T cells were
811 analysed by flow-cytometry. Specific killing was calculated as follows: (1-No. alive target
812 cells with TCE/No. alive target cells without TCE)*100. Cell morphology was assessed
813 with the light microscope Axio Vert.A1 (Zeiss) at 20x magnification.
814

815 *Design and production of the CD123CAR HDRT*
816 The CAR T cells were generated by co-electroporation of CRISPR-Cas9
817 Ribonucleoproteins (RNPs) specific for the *TRAC* locus and a double-stranded DNA HDR
818 template (HDRT). The HDRT encoding a second-generation CD123-specific CAR with
819 the scFv of clone CSL362, the CD8α hinge and transmembrane domain (Gen CD8A
820 ENSG00000153563), the intracellular signalling moieties 4-1BB (Gen TNFRSF9
821 ENSG00000049249) and CD3ζ (Gen CD247 ENSG00000198821), as well as the
822 fluorescent reporter protein GFP (for full sequence see Extended data table). It is flanked
823 by symmetric arms of homology (300 bp) complementary to the *TRAC* locus Exon 1. The

824 construct was synthesized by GenScript® and the plasmid was used as template for PCR
825 amplification (Kapa Hifi Hotstart Ready Mix, Cat#F-530-L, Roche). The PCR amplicon
826 was purified with NucleoSpin Gel and PCR clean-up kit (Macherey-Nagel) according to
827 the manufacturer's instruction and the correct size was verified by gel. The HDRT was
828 then condensed to a final concentration of 1µg/µl using vacuum concentration, and stored
829 at -20°C until usage.
830

831 *Engineering primary CD123CAR T cells.*
832 Protocols for human CRISPR/Cas9-mediated genome engineering are based on *Roth et*
833 *al.*[12,13] In short, Cas9 RNPs were freshly generated prior to each electroporation. Thawed
834 crRNA and tracrRNA (purchased from IDT Technologies, at 200µM) were mixed in a 1:1
835 molar ratio (120pmol each), denatured at 95°C for 5min, and annealed at room temperature
836 (RT) for 10 to 20min to complex a 80µM gRNA solution. Poly-Glutamic Acid (PGA; 15-
837 50 kDa at 100mg/ml; Sigma-Aldrich) was added to the gRNA in a 0.8:1 volume ratio[14]. To
838 complex RNPs, 60pmol recombinant Cas9 (University of California Berkeley at 40µM)
839 was mixed with the gRNA (molar ratio Cas9:gRNA = 1:2) and incubated for 20min at RT
840 in the dark. Prior to electroporation isolated human T cells were activated for 48h with
841 CD3/CD28 Dynabeads (Thermofisher) at a cell to beads ratio 1:1 together with the
842 recombinant human cytokines IL-2 (150U/ml), IL-7 (5ng/ml; R&D Systems) and IL-15
843 (5ng/ml; R&D systems). Electroporation was performed with the 4D-Nucleofector™
844 system (Lonza) with Program EH-115. Following activation, the T cells were de-beaded
845 using an EasySep™ magnet and $1x10^6$ cells were resuspended in 20µl Lonza supplemented
846 P3 electroporation buffer. HDRT (3-4µg) and RNPs (60pmol) were mixed separately and
847 incubated for 5min. The cells were added to the mix and the total volume was transferred

848 to the 16-well Nucleocuvette Strips. Immediately following electroporation 80µl of
849 prewarmed supplemented medium was added to each cuvette and incubated at 37°C. After
850 20min, the cells were transferred into 48-well culture plates and replenished wit IL-2
851 500U/ml. Following flow-sorting at day 3 to 5 post-electroporation the cells were expanded
852 for 5 to 6 days until used for the subsequent experiments. Control T cells were
853 electroporated with an incomplete RNP (missing the specific crRNA), otherwise processed
854 as the CAR T cells.
855

856 *In vitro human CD123CAR killing assay.*
857 The day before the co-culture HEK-293 target cells were stained with CTV and kept in
858 supplemented human medium overnight. The flow-sorted, expanded GFP^+ CAR T cells
859 and control cells were added to the target cells in an effector to target ratio 10:1 and co-
860 cultured for 24h. Specific killing and T cell activation was measured by flow cytometry.
861 Specific killing was calculated according to the indicated formula: (1-No. alive target cells
862 in co-culture with CAR T cells/No. alive target cells in co-culture with control cells)*100.
863 Using the microscope Axio Vert.A1 (Zeiss) cell morphology was recorded.
864

865 *In vitro 123CAR-mediated killing assay of non-virally engineered HSPCs.*
866 For the 123CAR killing assays the HSPCs were edited as described above. Two days
867 after electroporation edited HSPCs, MOLM-14-mCherry, OCI-AML2-mCherry, OCI-
868 AML3-mCherry or PDX (labelled with CTV according to the manufacturer's instruction)
869 were co-cultured with control T cells or 123CAR in a 96 U-bottom plate at an effector to
870 target ratio of 3:1 for 48 h at 37 °C. In a set of experiments MOLM-14-mCherry or PDX
871 (labelled with CTV according to the manufacturer's instruction) were co-cultured with

872 edited HSPCs and T cells or 123CAR cells at an effector to target to tumour ratio of
873 3:0.5:0.5 together. Cytotoxic activity (specific killing and elimination of non-edited
874 HSCs) was analysed by flow cytometry.
875

876 *Human cytokine measurement (ELISA)*
877 IFNγ was measured from the supernatants of the co-culture experiments (TCE / CAR)
878 using the colorimetric ELISA MAX Standard Set Human IFNγ kit (BioLegend) according
879 to the manufacturer's instruction. The optical density was read at 450 nm with the
880 microplate reader. A standard curve calculated from standard dilutions was run in
881 duplicates with every experiment.

882 *Genomic DNA extraction and sequencing from human T cells, eukaryotic cell lines and*
883 *HSPCs*
884 Genomic DNA was extracted using the QuickExtract™ (Biosearch technologies;
885 QE09050) according to the manufacturer's instruction. Alternatively, cells were lysed in
886 Tail Lysis Buffer (100 mM Tris [pH 8.5], 5 mM Na-EDTA, 0.2% SDS, 200 mM NaCl)
887 containing Proteinase K (0.1 µg; Sigma-Aldrich) at 56 °C (1000 rpm). The DNA was
888 precipitated with isopropanol (1:1 volume ratio), and washed in 70% ethanol. The genomic
889 DNA concentration was measured with a NanoDrop™ device (Thermo Fisher). PCR was
890 performed using either GoTaq G2 Green Master Mix (Cat#M782B, Promega) or Kapa Hifi
891 Hotstart Ready Mix. Sanger Sequencing was performed at Microsynth AG Switzerland.
892 Sequences were analysed using MegAlign Pro (DNASTAR).
893
894
895

896 *Next generation sequencing*

897 Genomic DNA was isolated from HSPCs using Quick extraction buffer. Targeted
898 amplicons library was prepared following Illumina's recommendation using a two-step
899 PCR protocol. Briefly, nested PCRs were performed on each DNA sample using the HiFi
900 KAPA polymerase (Roche). Following Illumina barcoding (Nextera indices, Illumina),
901 PCR samples were pooled, beads purified and quantified using Qubit dsDNA BR (Thermo
902 Fisher). Library was sequenced on an Illumina MiSeq instrument using Illumina MiSeq
903 Reagent Kit v2 Micro (300-cycles) with 50% PhiX spike-in (Illumina). After
904 demultiplexing, each sample was assessed for quality and analysed using CRISPResso v2
905 [REF 65]. For each of the samples, we provided the HDR template, the reference sequence, the
906 guide sequence and applied a minimum base quality of Phred 25. We used a custom R
907 script to quantify each allele within a quantification window of 4 nucleotides including one
908 silent mutation followed by the targeted AA.

909 *Bio-Layer Interferometry (BLI) measurement of binding*
910 All BLI measurements were performed either on an Octet Red96e (ForteBio) or on an Octet
911 R8 (Sartorius). The extracellular domain (ECD) of CD123 WT and variants were produced
912 and purified by Icosagen.

913 *CSL362 hIgG1 binding to CD123 WT ECD and variants*
914 Binding of antibody CSL362 hIgG1 to CD123 WT ECD and variants (analytes in solution)
915 was performed at low (50nM) and high (300nM) concentration of analyte. Antibody
916 CSL362 hIgG1 (captured ligand) was captured by Anti-Human Fc capture biosensor
917 (AHC) (Sartorius, PN: 18-5060) for 300s at 0.5µg/mL. Analytes CD123 WT ECD and
918 variants were titrated at 7 concentrations (1:2 dilution series) from 50nM to 0.78nM and
919 from 300nM to 4.7nM. Association to analyte was monitored for 300s and dissociation for

920 600s or 900s. Double reference subtraction was performed against buffer only and
921 biosensor loaded with a negative hIgG1 control. Regeneration was performed in 10mM
922 Gly-HCl pH1.7. Data were analysed using the Octet Data Analysis software HT 12.0. Data
923 were fitted to a 1:1 binding model. Kinetic rates k_a and k_d were globally fitted.

924 *6H6 mIgG1 binding to CD123 WT ECD and variants*
925 Binding of antibody 6H6 mIgG1 (Biolegend, PN: 306002; captured ligand) to CD123 WT
926 ECD and variants (analytes in solution) was performed using Streptavidin capture
927 biosensor (SA) (Sartorius, PN: 18-5019). CaptureSelect™ Biotin Anti-LC-kappa (Murine)
928 (Thermo Fischer, PN: 7103152100) was captured for 600s at 1µg/mL on SA tips. Those
929 biosensors were then used to capture antibody 6H6 mIgG1 for 300s at 2.5µg/mL. Analytes
930 CD123 WT ECD and variants were titrated at 7 concentrations from 50 to 1.56nM.
931 Association to analyte was monitored for 300s and dissociation for 600s. Buffer only well
932 was used as reference. Regeneration was performed in 10mM Gly-HCl pH1.7. Data were
933 analysed using the Octet Data Analysis software HT 12.0. Data were fitted (when possible)
934 to a 1:1 binding model. Kinetic rates k_a and k_d were globally fitted.

935 *IL-3 binding to CD123 WT ECD and variants*
936 Binding of IL-3 (Sino Biological, PN: 11858-H08H) (analyte in solution) to CD123 WT
937 ECD and variants (captured ligands) was performed using Streptavidin capture biosensor
938 (SA) (Sartorius, PN: 18-5019). CD123 WT ECD and variants were biotinylated using
939 Biotinylation kit Type B (Abcam, PN: ab201796) following manufacturer instructions.
940 Biotinylated CD123 WT ECD. and variants (ligands) were captured on SA tips for 1000s
941 at 3µg/mL concentration. Analyte IL-3 was titrated at 7 concentrations from 500 to 7.8nM
942 in PBS pH7.4. Association to analyte was monitored for 300s and dissociation for 120s.
943 Buffer only well was used as reference. No regeneration was performed, and a new set of

944 tips was used for each biotinylated captured ligand. Data were analysed using the Octet
945 Data Analysis software HT12.0. Due to the fast on/off nature of the interaction data were
946 analysed using Steady state analysis.
947

948 *Thermal stability analysis*
949 Differential Scanning Fluorimetry (DSF) analysis were performed on a Bio-Rad CFX96
950 Touch Deep Well RT PCR Detection System. Sypro Orange 5000X in DMSO (Sigma, PN:
951 S5692) was used at a final concentration of 5X. Temperature gradient was performed from
952 25 to 95°C in increment of 1.5°C in a reaction volume of 20µL. "FRET" scan mode was
953 used to monitor fluorescence. All samples were analysed at a final concentration of
954 0.25mg/mL in triplicate in PBS pH7.4. The temperature of protein unfolding transition
955 (Tm) was calculated using the 1st derivative method.
956

957 *Engineering of TF-1 cells expressing CD123 variants and functional assays thereof*
958 RNPs were freshly prepared as outlined above. 50pmol ssDNA HDRT (180bp length,
959 Ultramer DNA Oligonucleotides, synthetized by IDT) were added to the RNPs. Per
960 reaction $0.2x10^6$ TF-1 cells were re-suspended in 10µl R buffer (Neon™ Transfection
961 System) and electroporated using the Neon® Transfection System (1200V, 40ms, 1pulse).
962 Following an expansion period of 12 days the edited cells were flow sorted based on the
963 binding to MIRG123 and 6H6: WT ($MIRG123^+6H6^+$), KO ($MIRG123^-6H6^-$) and KI
964 ($MIRG123^-6H6^+$).
965 To test responsiveness of TF-1 cells to human IL-3, $0.18x10^5$ sorted cells were distributed
966 into white 96 well-plate clear bottom tissue-culture treated (Greiner) and different IL-3
967 concentrations indicated in **Fig. 5b** were added. In certain experiments MIRG123 was

968 added in the concentrations shown in **Fig. 5c**. After 3 days, proliferation was assessed using
969 CellTiter-Glo® 2.0 (Cat#G9241, Promega) according to the manufacturer's protocol.
970 Luminescence was assessed with the Synergy H1 (BioTek) with an integration time of 1s.
971

972 *Non-virally CRISPR/Cas9 mediated engineering of HSPCs*
973 Leukopaks were purchased from CytoCare and HSPCs were isolated by the LP-34 Process
974 using the CliniMACS Prodigy (Miltenyi). HSPCs were thawed in HSC-Brew GMP Basal
975 Medium (Miltenyi) supplemented with HSC-Brew GMP Supplement, 2% human serum
976 albumin, 100ng/mL Stem Cell Factor (SCF), 100ng/mL Thrombopoietin (TPO), 100ng/mL
977 Fms-like tyrosine kinase 3 ligand (Flt3L) and 60ng/mL IL-3 (Miltenyi) at a concentration
978 of $0.5x10^6$ cells/ml. Cells were electroporated 2 days later. gRNAs were freshly prepared
979 as outlined above, but 50 µM crRNA and tracrRNA were used to form the gRNA and
980 complexed with 1µM Spyfi Cas9 (Aldevron at 61.889 µM) at a molar ratio Cas9:gRNA =
981 1:2 and incubated for 20 min at RT. As control, incomplete RNPs lacking the site-specific
982 crRNA were generated. During the RNPs complexing, HSPCs were collected, washed
983 twice with electroporation buffer (Miltenyi) and resuspend in electroporation buffer at
984 $1x10^6$ cells/90 µl. Cells were then mixed with 5µl RNP and ssDNA HDRT encoding the
985 variants (5µl corresponding to 500pmol) and the whole volume was transferred into the
986 electroporation nucleocuvette. Electroporation was performed with the CliniMACS Prodigy
987 (600V 100µs burst / 400V 750µs square). Immediately after electroporation the cells were
988 transferred to a 6 well plate and rested for 20 minutes at RT. After 20min, 2mL of pre-
989 warmed HSC medium supplemented with 100ng/mL SCF, 100ng/mL TPO and 100ng/mL
990 Flt3L was added and the plate was incubated at 37°C.
991

992 *CD123 and CCR5 gene editing with CRISPR/Cas9 and rAAV6 virus*

993 *CD34$^+$ HSPC culture condition*
994 Plerixafor mobilized peripheral blood CD34$^+$ HSPCs were purchased from AllCells
995 (Alameda, CA, USA). The cells were thawed per manufacturer's instructions and were
996 cultured at 37°C, 5% CO2, and 5% O2. Cell culture medium was GMP SCGM medium
997 from CellGenix (Portsmouth, NH, USA) supplemented with human cytokine (PeproTech,
998 Rocky Hill, NJ, USA) cocktail containing SCF 100ng/ml, TPO 100ng/ml, Flt3L 100ng/ml,
999 and IL-6 100ng/ml. UM171 (35nM) (StemCell Technologies, Vancouver, Canada),
1000 streptomycin (20mg/ml) and penicillin (20U/ml) were added into the cell culture medium.

1001 *CD123 and CCR5 gene editing procedure*
1002 HSPCs were cultured and pre-stimulated for 72 hours after thaw and before gene editing.
1003 Chemically modified CD123 sgRNA and CCR5 sgRNA were synthesized by Synthego
1004 Corporation (Redwood City, CA, USA). SpyFi Cas9 was purchased from Aldevron, LLC
1005 (Fargo, ND, USA). CD123-E51K and CD123-E51T donor rAAV6 virus was purchased
1006 from SignaGen Laboratories (Frederick, MD, USA). CCR5-KO donor rAAV6 virus was
1007 produced in HEK-293T cells and was purified with AAVpro Purification Kit (TakaRa, San
1008 Jose, CA, USA). Electroporation of the RNP complex was performed using the Lonza 4D-
1009 Nucleofector (Lonza Group Ltd, Alpharetta, GA, USA) in P3 Primary Cell Solution with
1010 program DZ-100. Donor rAAV6 virus was immediately dispensed onto electroporated
1011 cells at multiplicity of infection (MOI) of $2.5x10^3$ vector genomes (vg) per cell for CD123
1012 and $5.0x10^3$ vg per cell for CCR5 based on the titres determined by ddPCR. The cells were
1013 then divided into two halves at $2.5x10^5$ cells/ml. One half was plated in SCGM medium
1014 supplemented with cytokines and 10ng/ml IL-3 (PeproTech, Rocky Hill, NJ, USA) as +IL-
1015 3 treatment. The other half was plated in SCGM medium supplemented with cytokines

1016 only as -IL-3 treatment. After incubation for 24 hours, a medium change was performed to
1017 remove residual rAAV6 virus. The $CD34^+$ HSPCs were cultured for up to 8 days for
1018 quantification of gene editing events, CFU assays and pSTAT5 staining and FACS
1019 analysis.
1020

1021 *Methylcellulose colony formation unit (CFU) assay of non-virally edited HSPCs*
1022 CFU assay was started at 72h post gene editing. For each condition, 1.1mL of semi-solid
1023 methylcellulose medium (StemCell Technologies) containing 500 cells were plated in a
1024 well of a SmartDish (StemCell Technologies) in duplicates. The cells were incubated at
1025 37 °C, 5% O2 and 5% CO2 for 14 days. The resulting progenitor colonies were counted
1026 and scored with STEMVision analysis (StemCell Technologies, Seattle, WA, USA) per
1027 manufacturer's instruction. Colonies were picked and subjected to sequencing. Shortly,
1028 colonies were washed with PBS and then resuspended in 25 µl DNA-QuickExtract
1029 solution. PCRs were performed and sent for sanger sequencing.

1030

1031 *Methylcellulose colony formation unit (CFU) assay of AAV-edited HSPCs*
1032 CFU assay was started at 48h post gene editing. For each condition, 1.1mL of semi-solid
1033 methylcellulose medium (StemCell Technologies, Seattle, WA, USA) containing 300 cells
1034 and with 10ng/ml IL-3 (+IL-3 treatment) or without IL-3 (-IL-3 treatment) were plated in
1035 a well of a SmartDish (StemCell Technologies, Seattle, WA, USA) in duplicates. The cells
1036 were incubated at 37 °C, 5% O2 and 5% CO2 for 14 days. The resulting progenitor colonies
1037 were counted and scored with STEMVision analysis (StemCell Technologies, Seattle, WA,
1038 USA) per manufacturer's instruction.
1039

1040 *pSTAT5 staining of non-virally edited HSPCs*
1041 On day 3 post gene editing, all cells were stimulated with 10ng/ml IL-3 for 1h at 37°C and
1042 then were subjected to pSTAT5 and CD123 staining. Briefly, after the 1h incubation, cells
1043 were fixed in 4% paraformaldehyde and then were permeabilized with ice-cold methanol.
1044 The permeabilized cells were stained with Alexa 647 mouse-anti-human Stat5 (pY694),
1045 BV650 mouse-anti-human CD123 clone 6H6 antibody and Alexa 488 MIRG123 in FACS
1046 buffer at RT for 1h. After staining, cells were washed with FACS buffer and then subjected
1047 for FACS analysis to Fortessa.
1048

1049 *pSTAT5 staining of AAV-edited HSPCs*
1050 On day 8 post gene editing, all cells were switched to growth medium without IL-3 for IL-
1051 3 starvation. After 1-day IL-3 starvation, for +IL-3 treatment, 10ng/ml IL-3 was added
1052 back to the cells which were originally cultured in +IL-3 medium. For -IL-3 treatment, IL-
1053 3 was not added into the cells which were originally cultured in -IL-3 medium. All cell
1054 cultures were incubated for 1h and then were subjected to pSTAT5 staining. Briefly, after
1055 1h incubation, cells were lysed and fixed in BD Phosflow Lyse/Fix Buffer and then were
1056 permeabilized with BD Phosflow Perm Buffer III (BD Biosciences, San Jose, CA, USA)
1057 following manufacturer's instruction. The permeabilized cells were stained with Alexa
1058 647 Mouse-anti-human Stat5 (pY694) antibody in PBS at RT for 1h. Alexa 647 Mouse
1059 isotype IgG (BD Pharmingen, San Jose, CA, USA) was used as a negative control. K-562
1060 cells which were not subjected to IL-3 treatment nor IL-3 stimulation was stained with the
1061 same pSTAT5 antibody as a positive control. After staining, cells were washed with PBS
1062 and then were subjected to CytoFLEX Flow Cytometer (Beckman Coulter Life Sciences,
1063 Brea, CA) for FACS analysis.

1064

1065 *Differentiation of non-virally edited HSPCs in vitro*

1066 Three days after electroporation cells were resuspended in StemPro media (Gibco)
1067 containing StemPro Nutrients, LDL 50ng/ml, P/S 1%, Glutamine 1%, Flt3 20ng/ml, TPO
1068 50ng/ml, IL-6 50ng/ml, IL-3 10ng/ml, IL-2 10ng/ml, IL-7 20ng/ml, EPO 3ng/ml, GM-CSF
1069 20ng/ml, SCF 100ng/ml, and 2000 cells/well were plated in a 96 round bottom well plate.
1070 In some wells, CSL-362-Tesirine at a concentration of 10ng/mL was added. After 14 days
1071 cells were collected, stained for CD33, GlyA/CD235a, CD14, CD15 and CD123 and
1072 acquired on a Fortessa.

1073

1074 *Mice*

1075 All animal work was performed in accordance with the federal and cantonal laws of
1076 Switzerland. Protocols were approved by the Animal Research Commission of the Canton
1077 of Basel-Stadt, Switzerland. All mice were housed in a specific pathogen-free (SPF)
1078 condition in accordance with institutional guidelines and ethical regulations. NBSGW
1079 (stock# 026622) female mice were purchased from Jackson Laboratories. The HSPCs were
1080 edited as described above. Two days after electroporation cells were collected and frozen
1081 in CS10 (Stem Cell Technologies). Cells were thawed at the day of injection, washed and
1082 resuspended in PBS at $10x10^6$ live cells/ml. Recipient NBSGW female mice (3 weeks old)
1083 were injected into the tail vein. Chimerism was analysed after 6 and 10 weeks in the blood
1084 by flow cytometry. Mice were euthanized 16 weeks after humanization.
1085 For secondary transplant, NSG-SGM3 (stock#013062) female mice were purchased from
1086 Jackson Laboratories. Mice were irradiated the day before BM transplant with 200cGy.
1087 Primary transplant mice were euthanized, bone marrow was isolated, and half of the bone

1088 marrow re-injected into the new host. Mice from secondary transplant were euthanized 8
1089 weeks after transplant.
1090

1091 *In vitro TCE-mediated killing assay of non-virally engineered HSPCs*
1092 For the TCE killing assays the HSPCs were edited as described above. Autologous human
1093 T cells were isolated from PBMCs as abovementioned and cultured overnight in
1094 supplemented media without stimulation. Two days after electroporation edited HSPCs
1095 were co-cultured in a 96 U-bottom plate together with human effector T cells at an effector
1096 to target ratio of 3:1 and the CD3/CSL362-TCE at 100ng/ml for 72 h at 37 °C. In a set of
1097 experiments MOLM-14 (labelled with CTV according to the manufacturer's instruction)
1098 were added to the autologous T cells and edited HSPCs at an effector to target to tumour
1099 ratio of 3:0.5:0.5 together with the CD3/CSL362-TCE (100ng/ml). Cytotoxic activity
1100 (specific killing and elimination of non-edited HSCs) was analysed by flow-cytometry.
1101 Specific killing was calculated as follows: (1-No. alive target cells with TCE/No. alive
1102 target cells without TCE)*100.
1103

1104 *Computational off-target prediction*
1105 The Cas-OFFinder algorithm [44] (release 2.4.1) was used to search the human reference
1106 genome hg38 for potential off-target sites in silico, using the following parameters:
1107 maximum number of mismatches = 3; maximum number of DNA bulges = 1; maximum
1108 number of RNA bulges = 1; PAM = NGG. The human genome reference hg38 (GRCh38
1109 Genome Reference Consortium Human Reference 38), was downloaded from the Golden
1110 Path repository at https://hgdownload.cse.ucsc.edu/goldenPath/hg38/chromosomes/. All
1111 chromosomes were used in the alignments. To account for redundant off-target sites,

1112 unique target regions were selected by grouping overlapping sites using bedtools cluster
1113 (v2.30.0) and selecting a representative alignment. The same off-target analysis was
1114 performed for two additional gRNAs targeting the VEGFA[45] and HBB[41,46] genes which
1115 served as benchmarks.
1116
1117 *Discover-Seq*
1118 Cells were nucleofected with an RNP complex to target either CD123 or BFP (used as a
1119 negative control). Thirteen hours after nucleofection, an aliquot of nucleofected cells were
1120 transferred to new media and genomic DNA was extracted 5 days later to check for genome
1121 editing efficiency. Ten million nucleofected cells were fixed in 1% formaldehyde at room
1122 temperature for 15 minutes. The fixation reaction was quenched with glycine to a final
1123 concentration of 125 mM. Cells were harvested and washed twice with chilled PBS and
1124 pellets were snap frozen and stored at -80° C until processing. To process, cell pellets were
1125 thawed on ice and incubated with lysis buffer 1 (LB) 1 (50 mM Hepes–KOH, pH 7.5; 140
1126 mM NaCl; 1 mM EDTA; 10% Glycerol; 0.5% NP-40 or Igepal CA-630; 0.25% Triton X-
1127 100; 1X protease inhibitors) on ice for 10 minutes. Cells were pelleted by centrifugation
1128 and incubated in LB 2 (10 mM Tris–HCL, pH8.0; 200 mM NaCl; 1 mM EDTA; 0.5 mM
1129 EDTA; 1X protease inhibitors) for 5 minutes on ice. The extracted nuclei were pelleted by
1130 centrifugation and resuspended in LB 3 (10mM Tris–HCl, pH8; 100mM NaCl; 1mM
1131 EDTA; 0.1% NaDeoxycholate; 0.5% N-lauroylsarcosine; 1X protease inhibitors). Nuclei
1132 were sonicated using a Covaris S2 sonicator with the following settings: duty cycle 5%,
1133 intensity 5, 200 cycles per burst, 7 minutes. Debris were pelleted by centrifugation at 4°C
1134 and the supernatant was transferred to a 5mL tube. 100µL of Dynabeads protein A that had

1135 been prebound with MRE11 antibody (Novus NB 100-142) were added to the cell lysate
1136 and samples were incubated at 4°C overnight with rotation. Beads were collected on a
1137 magnetic stand and washed with ice-cold RIPA buffer 6 times, followed by a final wash
1138 with TBS before resuspending beads in 200 µL of elution buffer (50 mM Tris–HCl, pH 8;
1139 10 mM EDTA; 1% SDS). The bead slurries were incubated overnight at 65°C to reverse
1140 crosslinks. Samples were treated with 1 mg/mL RNaseA (Ambion, catalog 2271) for 30
1141 minutes at 37°C, followed by proteinase K treatment 20 mg/mL
1142 (Invitrogen, catalog 25530-049) for 1 hour at 55°C. DNA was then purified using a
1143 MinElute PCR Purification Kit (Qiagen, catalog #28004) and sequencing libraries were
1144 prepared using a NEBNext Ultra II kit (NEB, catalog E7645L). Samples were sequenced
1145 with 50-bp paired-end reads on an Illumina NextSeq at a depth of 30 million reads per
1146 sample. Following sequencing, data was analysed using the BLENDER2 pipeline
1147 (available on GitHub).
1148
1149 *rhAmpSeq*
1150 Validation of off-target sites was performed using the RNase H-dependent amplification
1151 and sequencing (rhAmpSeq) system from IDT. rhAmpSeq primer panels for targeted
1152 amplification were generated using the rhAmpSeq design tool defining the insert size
1153 between 150-250bp. rhAmpSeq CRISPR library was prepared according to manufacturer's
1154 instructions and sequenced on an Illumina MiniSeq instrument (MiniSeq Mid Output Kit,
1155 300-cycles). Sequencing data were analysed with the rhAmpSeq CRISPR Analysis tool
1156 from IDT using the default settings.
1157

1158 *CAST-Seq*

1159 Cells were nucleofected with RNP complexes to target CD123. Genomic DNA was
1160 extracted 5 days later using the NucleoSpin Tissue kit (Machery and Nagel). CAST-Seq
1161 library preparations were performed as described[42], and data analysed using an improved
1162 bioinformatics pipeline[43].

1163

1164 *Statistical Analysis*
1165 Statistical Analysis was performed on Prism 9.1.2 software (GraphPad). Number of
1166 donors and replicates are found within each figure legend.

1167 **References**

1168 1 Carter, P. J. & Rajpal, A. Designing antibodies as therapeutics. *Cell* **185**, 2789-
1169 2805, doi:10.1016/j.cell.2022.05.029 (2022).
1170 2 Globerson Levin, A., Riviere, I., Eshhar, Z. & Sadelain, M. CAR T cells:
1171 Building on the CD19 paradigm. *Eur J Immunol* **51**, 2151-2163,
1172 doi:10.1002/eji.202049064 (2021).
1173 3 June, C. H., O'Connor, R. S., Kawalekar, O. U., Ghassemi, S. & Milone, M. C.
1174 CAR T cell immunotherapy for human cancer. *Science* **359**, 1361-1365,
1175 doi:10.1126/science.aar6711 (2018).
1176 4 Lee, D. W. *et al.* T cells expressing CD19 chimeric antigen receptors for acute
1177 lymphoblastic leukaemia in children and young adults: a phase 1 dose-escalation
1178 trial. *Lancet* **385**, 517-528, doi:10.1016/S0140-6736(14)61403-3 (2015).
1179 5 Kochenderfer, J. N. *et al.* Eradication of B-lineage cells and regression of
1180 lymphoma in a patient treated with autologous T cells genetically engineered to
1181 recognize CD19. *Blood* **116**, 4099-4102, doi:10.1182/blood-2010-04-281931
1182 (2010).
1183 6 Brentjens, R. J. *et al.* Safety and persistence of adoptively transferred autologous
1184 CD19-targeted T cells in patients with relapsed or chemotherapy refractory B-cell
1185 leukemias. *Blood* **118**, 4817-4828, doi:10.1182/blood-2011-04-348540 (2011).
1186 7 Kalos, M. *et al.* T cells with chimeric antigen receptors have potent antitumor
1187 effects and can establish memory in patients with advanced leukemia. *Sci Transl*
1188 *Med* **3**, 95ra73, doi:10.1126/scitranslmed.3002842 (2011).
1189 8 Mougiakakos, D. *et al.* CD19-Targeted CAR T Cells in Refractory Systemic
1190 Lupus Erythematosus. *N Engl J Med* **385**, 567-569, doi:10.1056/NEJMc2107725
1191 (2021).
1192 9 Porter, D. L., Levine, B. L., Kalos, M., Bagg, A. & June, C. H. Chimeric antigen
1193 receptor-modified T cells in chronic lymphoid leukemia. *N Engl J Med* **365**, 725-
1194 733, doi:10.1056/NEJMoa1103849 (2011).
1195 10 Paszkiewicz, P. J. *et al.* Targeted antibody-mediated depletion of murine CD19
1196 CAR T cells permanently reverses B cell aplasia. *J Clin Invest* **126**, 4262-4272,
1197 doi:10.1172/JCI84813 (2016).
1198 11 Finck, A. V., Blanchard, T., Roselle, C. P., Golinelli, G. & June, C. H. Engineered
1199 cellular immunotherapies in cancer and beyond. *Nat Med* **28**, 678-689,
1200 doi:10.1038/s41591-022-01765-8 (2022).
1201 12 Majzner, R. G. & Mackall, C. L. Clinical lessons learned from the first leg of the
1202 CAR T cell journey. *Nat Med* **25**, 1341-1355, doi:10.1038/s41591-019-0564-6
1203 (2019).
1204 13 Eyquem, J. *et al.* Targeting a CAR to the TRAC locus with CRISPR/Cas9
1205 enhances tumour rejection. *Nature* **543**, 113-117, doi:10.1038/nature21405
1206 (2017).
1207 14 Lynn, R. C. *et al.* c-Jun overexpression in CAR T cells induces exhaustion
1208 resistance. *Nature* **576**, 293-300, doi:10.1038/s41586-019-1805-z (2019).
1209 15 Maude, S. L. *et al.* Chimeric antigen receptor T cells for sustained remissions in
1210 leukemia. *N Engl J Med* **371**, 1507-1517, doi:10.1056/NEJMoa1407222 (2014).

1211 16 Melenhorst, J. J. *et al.* Decade-long leukaemia remissions with persistence of
1212 CD4(+) CAR T cells. *Nature* **602**, 503-509, doi:10.1038/s41586-021-04390-6
1213 (2022).
1214 17 Perna, F. *et al.* Integrating Proteomics and Transcriptomics for Systematic
1215 Combinatorial Chimeric Antigen Receptor Therapy of AML. *Cancer Cell* **32**,
1216 506-519 e505, doi:10.1016/j.ccell.2017.09.004 (2017).
1217 18 Haubner, S. *et al.* Coexpression profile of leukemic stem cell markers for
1218 combinatorial targeted therapy in AML. *Leukemia* **33**, 64-74,
1219 doi:10.1038/s41375-018-0180-3 (2019).
1220 19 Baroni, M. L. *et al.* 41BB-based and CD28-based CD123-redirected T-cells ablate
1221 human normal hematopoiesis in vivo. *J Immunother Cancer* **8**, doi:10.1136/jitc-
1222 2020-000845 (2020).
1223 20 Zeng, A. G. X. *et al.* A cellular hierarchy framework for understanding
1224 heterogeneity and predicting drug response in acute myeloid leukemia. *Nat Med*
1225 **28**, 1212-1223, doi:10.1038/s41591-022-01819-x (2022).
1226 21 Gill, S. *et al.* Preclinical targeting of human acute myeloid leukemia and
1227 myeloablation using chimeric antigen receptor-modified T cells. *Blood* **123**, 2343-
1228 2354, doi:10.1182/blood-2013-09-529537 (2014).
1229 22 Irving, M., Zoete, V., Bassani-Sternberg, M. & Coukos, G. A roadmap for driving
1230 CAR T cells toward the oncogenic immunopeptidome. *Cancer Cell* **40**, 20-22,
1231 doi:10.1016/j.ccell.2021.12.011 (2022).
1232 23 Mause, E. R. V., Atanackovic, D., Lim, C. S. & Luetkens, T. Roadmap to
1233 affinity-tuned antibodies for enhanced chimeric antigen receptor T cell function
1234 and selectivity. *Trends Biotechnol* **40**, 875-890, doi:10.1016/j.tibtech.2021.12.009
1235 (2022).
1236 24 Arai, Y. *et al.* Myeloid Conditioning with c-kit-Targeted CAR-T Cells Enables
1237 Donor Stem Cell Engraftment. *Mol Ther* **26**, 1181-1197,
1238 doi:10.1016/j.ymthe.2018.03.003 (2018).
1239 25 Myburgh, R. *et al.* Anti-human CD117 CAR T-cells efficiently eliminate healthy
1240 and malignant CD117-expressing hematopoietic cells. *Leukemia* **34**, 2688-2703,
1241 doi:10.1038/s41375-020-0818-9 (2020).
1242 26 Majzner, R. G. & Mackall, C. L. Tumor Antigen Escape from CAR T-cell
1243 Therapy. *Cancer Discov* **8**, 1219-1226, doi:10.1158/2159-8290.CD-18-0442
1244 (2018).
1245 27 Kim, M. Y. *et al.* Genetic Inactivation of CD33 in Hematopoietic Stem Cells to
1246 Enable CAR T Cell Immunotherapy for Acute Myeloid Leukemia. *Cell* **173**,
1247 1439-1453 e1419, doi:10.1016/j.cell.2018.05.013 (2018).
1248 28 Borot, F. *et al.* Gene-edited stem cells enable CD33-directed immune therapy for
1249 myeloid malignancies. *Proc Natl Acad Sci U S A* **116**, 11978-11987,
1250 doi:10.1073/pnas.1819992116 (2019).
1251 29 Humbert, O. *et al.* Engineering resistance to CD33-targeted immunotherapy in
1252 normal hematopoiesis by CRISPR/Cas9-deletion of CD33 exon 2. *Leukemia* **33**,
1253 762-808, doi:10.1038/s41375-018-0277-8 (2019).
1254 30 Emerson, S. G., Yang, Y. C., Clark, S. C. & Long, M. W. Human recombinant
1255 granulocyte-macrophage colony stimulating factor and interleukin 3 have

1256 overlapping but distinct hematopoietic activities. *J Clin Invest* **82**, 1282-1287,
1257 doi:10.1172/JCI113727 (1988).
1258 31 Jordan, C. T. *et al.* The interleukin-3 receptor alpha chain is a unique marker for
1259 human acute myelogenous leukemia stem cells. *Leukemia* **14**, 1777-1784,
1260 doi:10.1038/sj.leu.2401903 (2000).
1261 32 Liu, T. F. *et al.* Diphtheria toxin fused to variant interleukin-3 provides enhanced
1262 binding to the interleukin-3 receptor and more potent leukemia cell cytotoxicity.
1263 *Exp Hematol* **32**, 277-281, doi:10.1016/j.exphem.2003.11.010 (2004).
1264 33 Roberts, A. W. *et al.* A phase I study of anti-CD123 monocional antibody (mAb)
1265 CSL360 targeting leukemia stem cells (LSC) in AML. *J Clin Oncol* **28**, doi:DOI
1266 10.1200/jco.2010.28.15_suppl.e13012 (2010).
1267 34 Busfield, S. J. *et al.* Targeting of acute myeloid leukemia in vitro and in vivo with
1268 an anti-CD123 mAb engineered for optimal ADCC. *Leukemia* **28**, 2213-2221,
1269 doi:10.1038/leu.2014.128 (2014).
1270 35 Kovtun, Y. *et al.* A CD123-targeting antibody-drug conjugate, IMGN632,
1271 designed to eradicate AML while sparing normal bone marrow cells. *Blood Adv* **2**,
1272 848-858, doi:10.1182/bloodadvances.2018017517 (2018).
1273 36 Chichili, G. R. *et al.* A CD3xCD123 bispecific DART for redirecting host T cells
1274 to myelogenous leukemia: preclinical activity and safety in nonhuman primates.
1275 *Sci Transl Med* **7**, 289ra282, doi:10.1126/scitranslmed.aaa5693 (2015).
1276 37 Hutmacher, C. *et al.* Development of a novel fully-human anti-CD123 antibody to
1277 target acute myeloid leukemia. *Leuk Res* **84**, 106178,
1278 doi:10.1016/j.leukres.2019.106178 (2019).
1279 38 Broughton, S. E. *et al.* Dual mechanism of interleukin-3 receptor blockade by an
1280 anti-cancer antibody. *Cell Rep* **8**, 410-419, doi:10.1016/j.celrep.2014.06.038
1281 (2014).
1282 39 Strohl, W. R. & Naso, M. Bispecific T-Cell Redirection versus Chimeric Antigen
1283 Receptor (CAR)-T Cells as Approaches to Kill Cancer Cells. *Antibodies (Basel)*
1284 **8**, doi:10.3390/antib8030041 (2019).
1285 40 Kitamura, T. *et al.* Establishment and characterization of a unique human cell line
1286 that proliferates dependently on GM-CSF, IL-3, or erythropoietin. *J Cell Physiol*
1287 **140**, 323-334, doi:10.1002/jcp.1041400219 (1989).
1288 41 Wienert, B. *et al.* Unbiased detection of CRISPR off-targets in vivo using
1289 DISCOVER-Seq. *Science* **364**, 286-289, doi:10.1126/science.aav9023 (2019).
1290 42 Turchiano, G. *et al.* Quantitative evaluation of chromosomal rearrangements in
1291 gene-edited human stem cells by CAST-Seq. *Cell Stem Cell* **28**, 1136-1147
1292 e1135, doi:10.1016/j.stem.2021.02.002 (2021).
1293 43 Rhiel, M. *et al.* T-CAST: An optimized CAST-Seq pipeline for TALEN confirms
1294 superior safety and efficacy of obligate-heterodimeric scaffolds. *Front Genome*
1295 *Ed* **5**, 1130736, doi:10.3389/fgeed.2023.1130736 (2023).
1296 44 Bae, S., Park, J. & Kim, J. S. Cas-OFFinder: a fast and versatile algorithm that
1297 searches for potential off-target sites of Cas9 RNA-guided endonucleases.
1298 *Bioinformatics* **30**, 1473-1475, doi:10.1093/bioinformatics/btu048 (2014).
1299 45 Chaudhari, H. G. *et al.* Evaluation of Homology-Independent CRISPR-Cas9 Off-
1300 Target Assessment Methods. *CRISPR J* **3**, 440-453, doi:10.1089/crispr.2020.0053
1301 (2020).

1302 46 DeWitt, M. A. *et al.* Selection-free genome editing of the sickle mutation in
1303 human adult hematopoietic stem/progenitor cells. *Science Translational Medicine*
1304 **8**, doi:ARTN 360ra134
1305 10.1126/scitranslmed.aaf9336 (2016).
1306 47 Czechowicz, A., Kraft, D., Weissman, I. L. & Bhattacharya, D. Efficient
1307 transplantation via antibody-based clearance of hematopoietic stem cell niches.
1308 *Science* **318**, 1296-1299, doi:10.1126/science.1149726 (2007).
1309 48 Palchaudhuri, R. *et al.* Non-genotoxic conditioning for hematopoietic stem cell
1310 transplantation using a hematopoietic-cell-specific internalizing immunotoxin.
1311 *Nat Biotechnol* **34**, 738-745, doi:10.1038/nbt.3584 (2016).
1312 49 Li, Z., Czechowicz, A., Scheck, A., Rossi, D. J. & Murphy, P. M. Hematopoietic
1313 chimerism and donor-specific skin allograft tolerance after non-genotoxic CD117
1314 antibody-drug-conjugate conditioning in MHC-mismatched allotransplantation.
1315 *Nat Commun* **10**, 616, doi:10.1038/s41467-018-08202-w (2019).
1316 50 Czechowicz, A. *et al.* Selective hematopoietic stem cell ablation using CD117-
1317 antibody-drug-conjugates enables safe and effective transplantation with
1318 immunity preservation. *Nat Commun* **10**, 617, doi:10.1038/s41467-018-08201-x
1319 (2019).
1320 51 Chiesa, R. *et al.* Base-Edited CAR7 T Cells for Relapsed T-Cell Acute
1321 Lymphoblastic Leukemia. *N Engl J Med*, doi:10.1056/NEJMoa2300709 (2023).
1322 52 Kornete, M., Marone, R. & Jeker, L. T. Highly Efficient and Versatile Plasmid-
1323 Based Gene Editing in Primary T Cells. *J Immunol* **200**, 2489-2501,
1324 doi:10.4049/jimmunol.1701121 (2018).
1325 53 Dever, D. P. *et al.* CRISPR/Cas9 beta-globin gene targeting in human
1326 haematopoietic stem cells. *Nature* **539**, 384-389, doi:10.1038/nature20134 (2016).
1327 54 Cromer, M. K. *et al.* Ultra-deep sequencing validates safety of CRISPR/Cas9
1328 genome editing in human hematopoietic stem and progenitor cells. *Nat Commun*
1329 **13**, 4724, doi:10.1038/s41467-022-32233-z (2022).
1330 55 Anzalone, A. V., Koblan, L. W. & Liu, D. R. Genome editing with CRISPR-Cas
1331 nucleases, base editors, transposases and prime editors. *Nat Biotechnol* **38**, 824-
1332 844, doi:10.1038/s41587-020-0561-9 (2020).
1333 56 Everette, K. A. *et al.* Ex vivo prime editing of patient haematopoietic stem cells
1334 rescues sickle-cell disease phenotypes after engraftment in mice. *Nat Biomed Eng*
1335 **7**, 616-628, doi:10.1038/s41551-023-01026-0 (2023).
1336 57 Kim, L. *et al.* Acute cardiotoxicity after initiation of the novel tyrosine kinase
1337 inhibitor gilteritinib for acute myeloid leukemia. *Cardiooncology* **7**, 36,
1338 doi:10.1186/s40959-021-00122-x (2021).
1339 58 Pfister, O. *et al.* FLT3 activation improves post-myocardial infarction remodeling
1340 involving a cytoprotective effect on cardiomyocytes. *J Am Coll Cardiol* **63**, 1011-
1341 1019, doi:10.1016/j.jacc.2013.08.1647 (2014).
1342 59 Niswander, L. M. *et al.* Potent preclinical activity of FLT3-directed chimeric
1343 antigen receptor T-cell immunotherapy against FLT3- mutant acute myeloid
1344 leukemia and KMT2A-rearranged acute lymphoblastic leukemia. *Haematologica*
1345 **108**, 457-471, doi:10.3324/haematol.2022.281456 (2023).

1346 60 Asano, T. *et al.* X-linked recessive TLR7 deficiency in ~1% of men under 60
1347 years old with life-threatening COVID-19. *Sci Immunol* **6**,
1348 doi:10.1126/sciimmunol.abl4348 (2021).
1349 61 Persaud, S. P. *et al.* Antibody-drug conjugates plus Janus kinase inhibitors enable
1350 MHC-mismatched allogeneic hematopoietic stem cell transplantation. *J Clin*
1351 *Invest* **131**, doi:10.1172/JCI145501 (2021).
1352 62 Saha, A. *et al.* A CD45-targeted antibody-drug conjugate successfully conditions
1353 for allogeneic hematopoietic stem cell transplantation in mice. *Blood* **139**, 1743-
1354 1759, doi:10.1182/blood.2021012366 (2022).
1355 63 Sabatier, M. *et al.* C/EBPa confers dependence to fatty acid anabolic pathways
1356 and vulnerability to lipid oxidative stress-induced ferroptosis in FLT3-mutant
1357 leukemia. *Cancer Discov*, doi:10.1158/2159-8290.CD-22-0411 (2023).
1358 64 Larrue, C. *et al.* Mitochondrial fusion is a therapeutic vulnerability of acute
1359 myeloid leukemia. *Leukemia* **37**, 765-775, doi:10.1038/s41375-023-01835-x
1360 (2023).
1361 65 Clement, K. *et al.* CRISPResso2 provides accurate and rapid genome editing
1362 sequence analysis. *Nat Biotechnol* **37**, 224-226, doi:10.1038/s41587-019-0032-3
1363 (2019).
1364

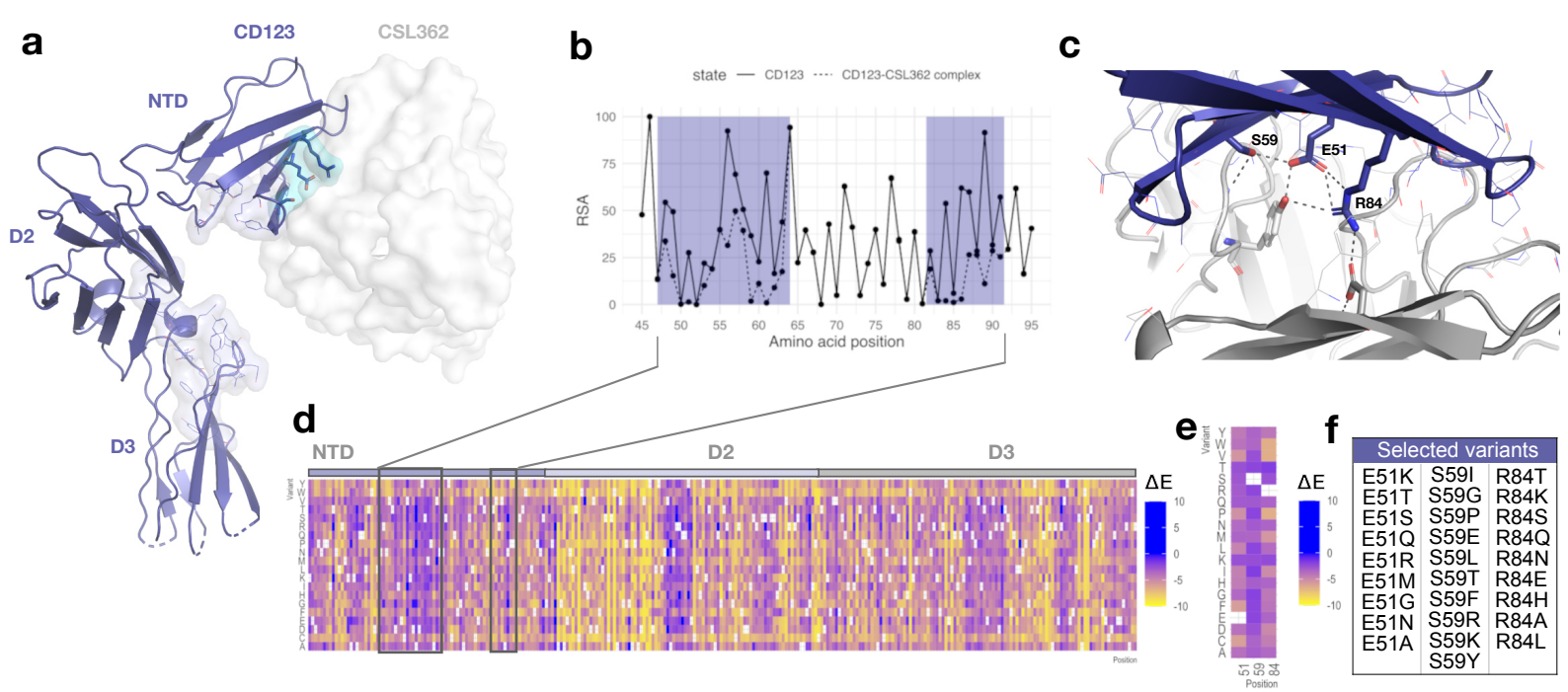

Figure 1. Rational design of human CD123 protein variants to shield from targeted immunotherapy

a, Crystal structure of the CD123-CSL362 complex in open conformation (PDB ID: 4JZJ[38]). CD123 is shown as ribbons. The CSL362 antibody variable domain is shown as white surface. CD123 amino acid residues involved in IL-3 binding are highlighted as lines and in light-blue. **b**, Per-residue relative solvent accessibility (RSA) computed on the CSL362-free (solid line) and CSL362-bound (dashed line) states based on the X-ray structure of the CD123-CSL362 complex (PDB ID: 4JZJ). RSA data are shown for the N-terminal domain. The CSL362 epitope region is highlighted by blue rectangles. **c**, Amino acid residues at the interface of the CD123-CSL362 complex are highlighted as lines and sticks. Side chain mediated intermolecular contacts are shown as dashed black lines. **d**, The predicted ΔE mutational landscape of CD123 is shown as a heatmap for the full extracellular domain (residue range 20-305, x-axis) and **e**, selected amino acid positions: E51, S59 and R84. Heatmap color ranges from yellow (ΔE <0, predicted damaging) to blue (ΔE ≥0, predicted neutral or beneficial). **f**, Selected amino acid variants at residues E51, S59, R84 sorted by decreasing ΔE values.

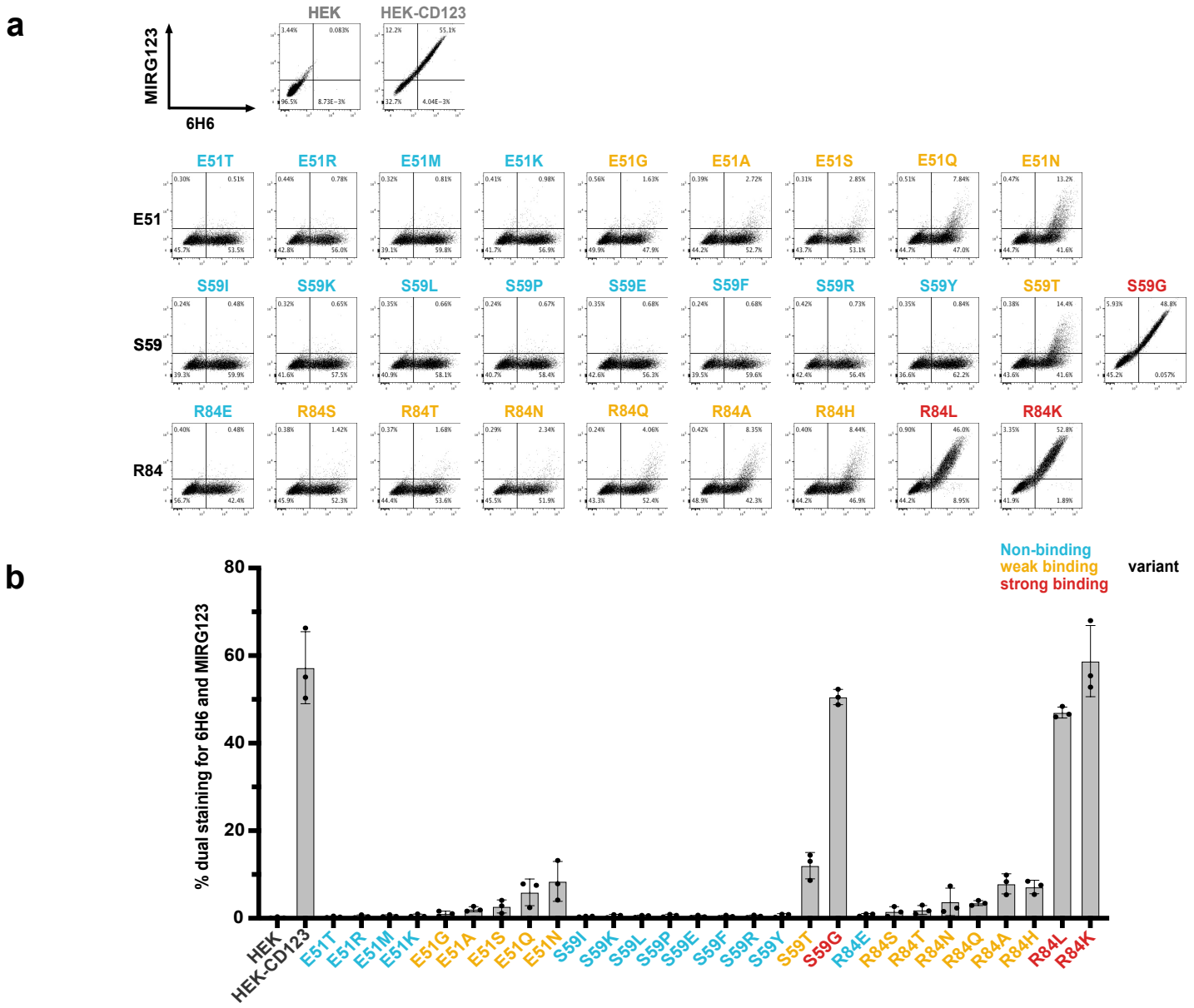

Figure 2: Preserved expression of engineered CD123 variants despite abolished binding to the monoclonal antibody MIRG123

a, Flow cytometry plots and **b,** summarizing bar graph showing binding of the anti-human CD123 antibody MIRG123 (biosimilar of CSL362) and the control clone 6H6 to wildtype CD123 and its 28 variants stably expressed in HEK-293 cells. Variants were categorized based on the dual staining to MIRG123 and 6H6 as non-binding (blue, <1% dual staining), weak (orange, 1-20%) or strong (red, >20%) binding variants. Control conditions (grey) are HEK-293 cells stably expressing wildtype CD123 (HEK-CD123) and non-transduced HEK-293 cells (HEK). Error bars: mean ± SD. Each symbol represents an individual experiment. Data in **a** is representative of three independent experiments.

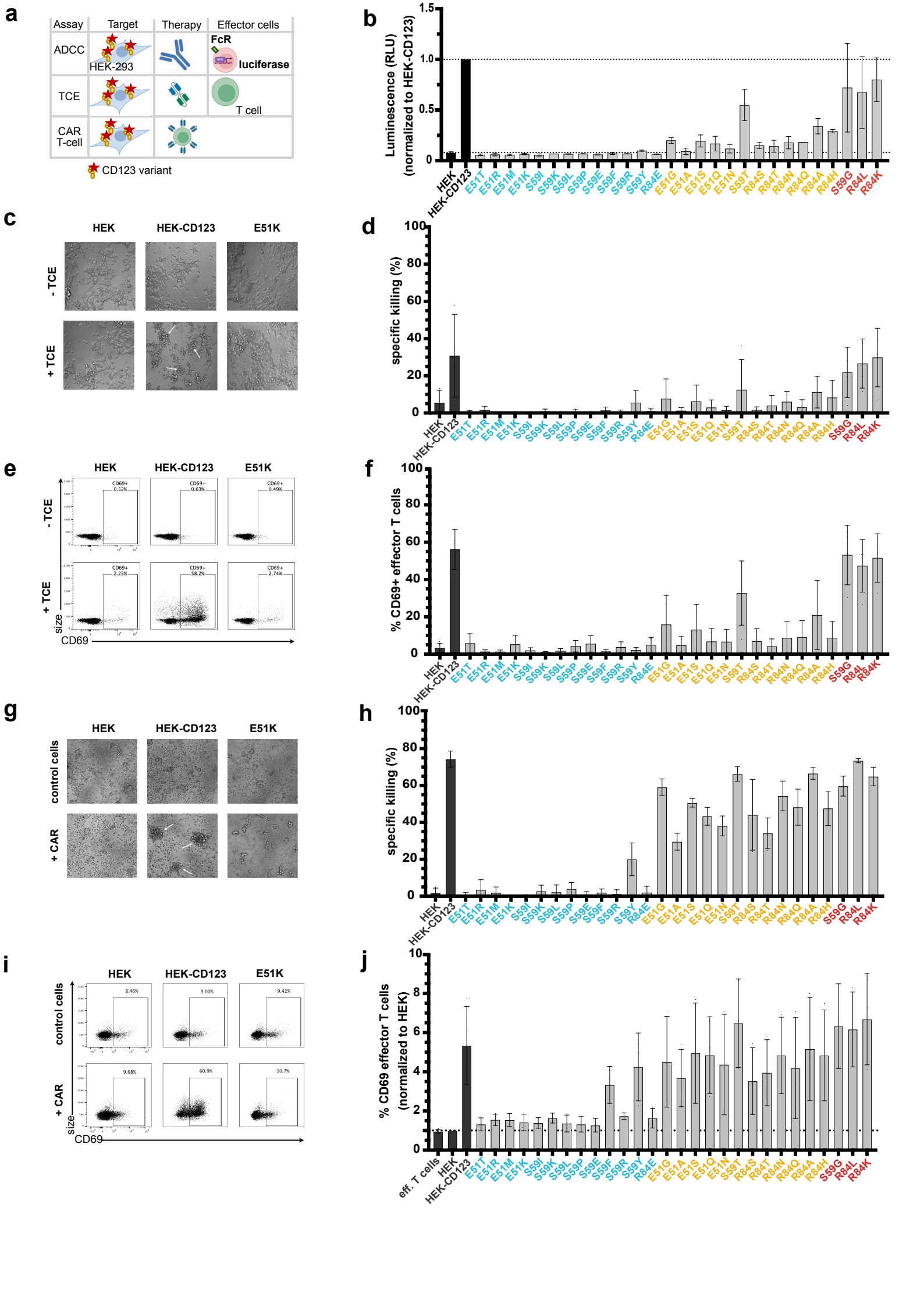
a
Assay
Target
Therapy
Effector cells
ADCC
HEK-293
FcR
luciferase
TCE
T cell
CAR T-cell
CD123 variant
b
Luminescence (RLU) (normalized to HEK-CD123)
c
HEK
HEK-CD123
E51K
- TCE
+ TCE
d
specific killing (%)
e
CD69+ 0.52%
CD69+ 0.63%
CD69+ 0.49%
CD69+ 2.23%
CD69+ 58.2%
CD69+ 2.74%
size
CD69
f
% CD69+ effector T cells
g
control cells
+ CAR
h
specific killing (%)
i
8.46%
9.00%
9.42%
9.68%
60.9%
10.7%
j
% CD69 effector T cells (normalized to HEK)
eff. T cells
HEK
HEK-CD123
E51T
E51R
E51M
E51K
S59I
S59K
S59L
S59P
S59E
S59F
S59R
S59Y
R84E
E51G
E51A
E51S
E51Q
E51N
S59T
R84S
R84T
R84N
R84Q
R84A
R84H
S59G
R84L
R84K

Figure 3: Cells expressing engineered CD123 variants are shielded from multiple targeted immunotherapy modalities *in vitro*

a, Schematic to assess shielding of CD123 expressing cells from three targeted immunotherapies (ADCC, TCE, CAR T-cell) in vitro. **b,** MIRG123-induced ADCC measured by luminescence of the effector cell line Jurkat/FcγRIIIa/NFAT-Luc following co-culture with HEK, HEK-CD123 or the CD123 variants. Luminescence signal normalized to the culture with HEK-CD123 (top dashed line). Data of 2 independent experiments. **c-f,** 3-day co-culture of effector T cells and HEK-293 expressing CD123 and its variants with and without CSL362/OKT3-TCE (TCE). Data represent 5 independent blood donors and experiments with 2 technical replicates per group. **c,** Representative images (Magnification 20x) after 3-day co-culture with HEK, HEK-CD123 or E51K with and without TCE. White arrows indicate cell clustering. **d,** Specific TCE-mediated killing of HEK-293 cells or its variants. **e,** Representative flow cytometry plots indicating CD69-expression in effector T cells without (top) and with (bottom) TCE after 3 days co-cultures with HEK, HEK-CD123 and the variant E51K. **f,** Frequency of CD69-expressing $CD3^+$ effector T cells after 3 days. **g-j,** Human 123CAR T cells were co-cultured with the target cells HEK, HEK-CD123 or its variants for 24h. Control T cells were electroporated with an HDRT, but incomplete RNP. Data from 3 independent blood donors and experiments with 2 technical replicates per group. **g,** Representative microscopy images (Magnification 20x) after 1 day with white arrows indicating cell clustering. **h,** Specific killing of target cells measured by flow cytometry at day 1 of co-culture. **i,** Representative FACS plots and **j,** summary of $CD69^+$ 123CAR T cells either alone (effector T cells) or in the presence of HEK, HEK-CD123 or all CD123 variants after 24h co-culture. The data are normalized to %$CD69^+$cells in the presence of HEK target cells.
b-j, Error bars: mean ± SD.

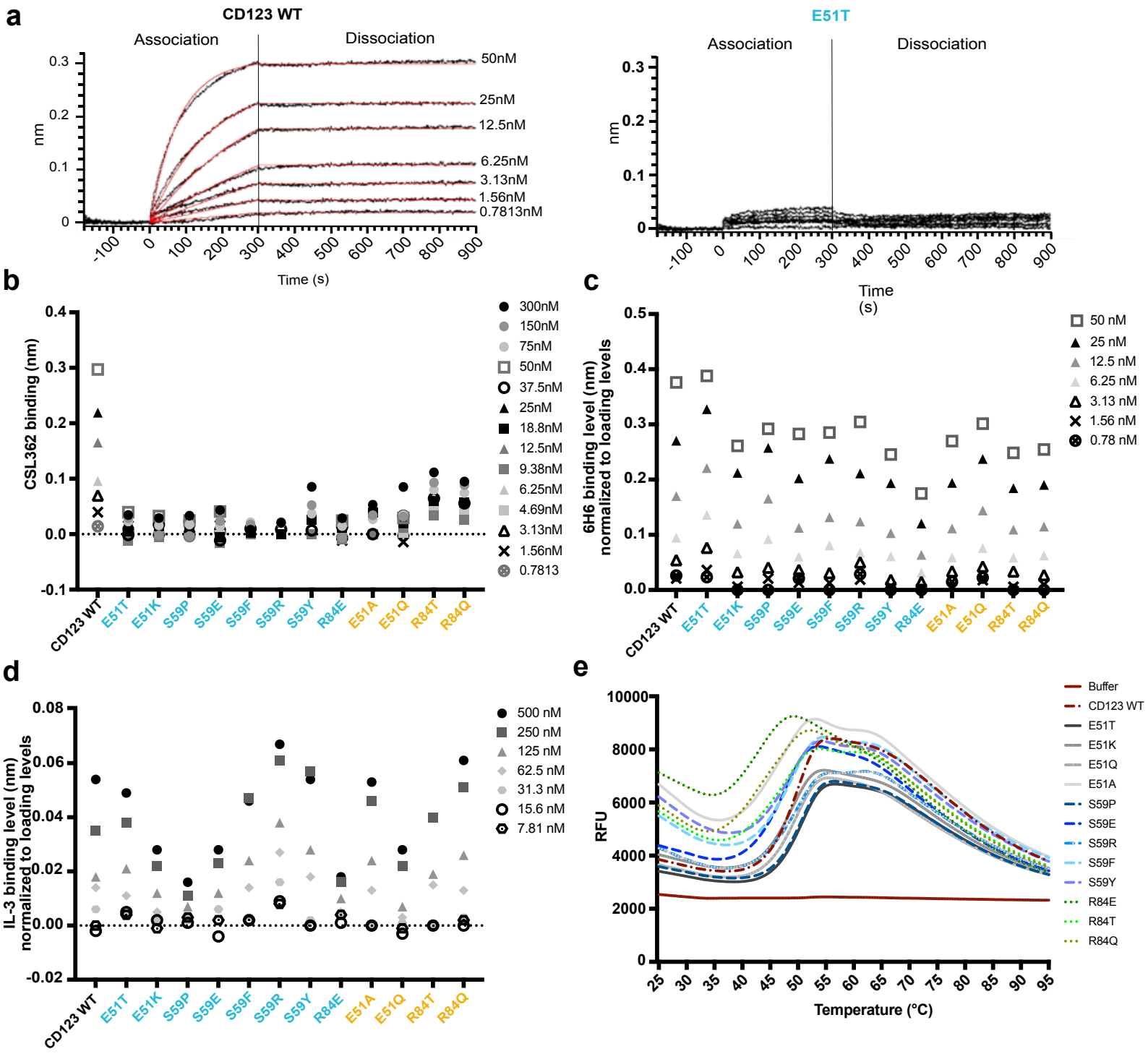

Figure 4. Biophysical characterization of selected CD123 protein variants

a, Binding of CSL362 to recombinant extracellular domain (ECD) of CD123 WT (**left**) and CD123 E51T (**right**) at increasing concentrations measured of CSL362 by Bio-Layer Interferometry. **b**, Binding levels of CD123 WT and its variants at different concentrations to captured CSL362 at 280s. CD123 WT reaches its saturation to CSL362 at 50nM, therefore higher concentrations were not measured. **c,** Binding levels of CD123 WT and its variants to the captured antibody 6H6 (normalized to the loading level of 6H6) at 250s. **d,** Binding levels of IL-3 to biotinylated CD123 WT and variants (normalized to loading levels of biotinylated CD123 WT and its variants) at 250s. **e,** Thermal unfolding (Relative Fluorescence Unit, RFU) of CD123 WT and variants measured by Differential Scanning Fluorimetry (DSF) with increasing temperatures.

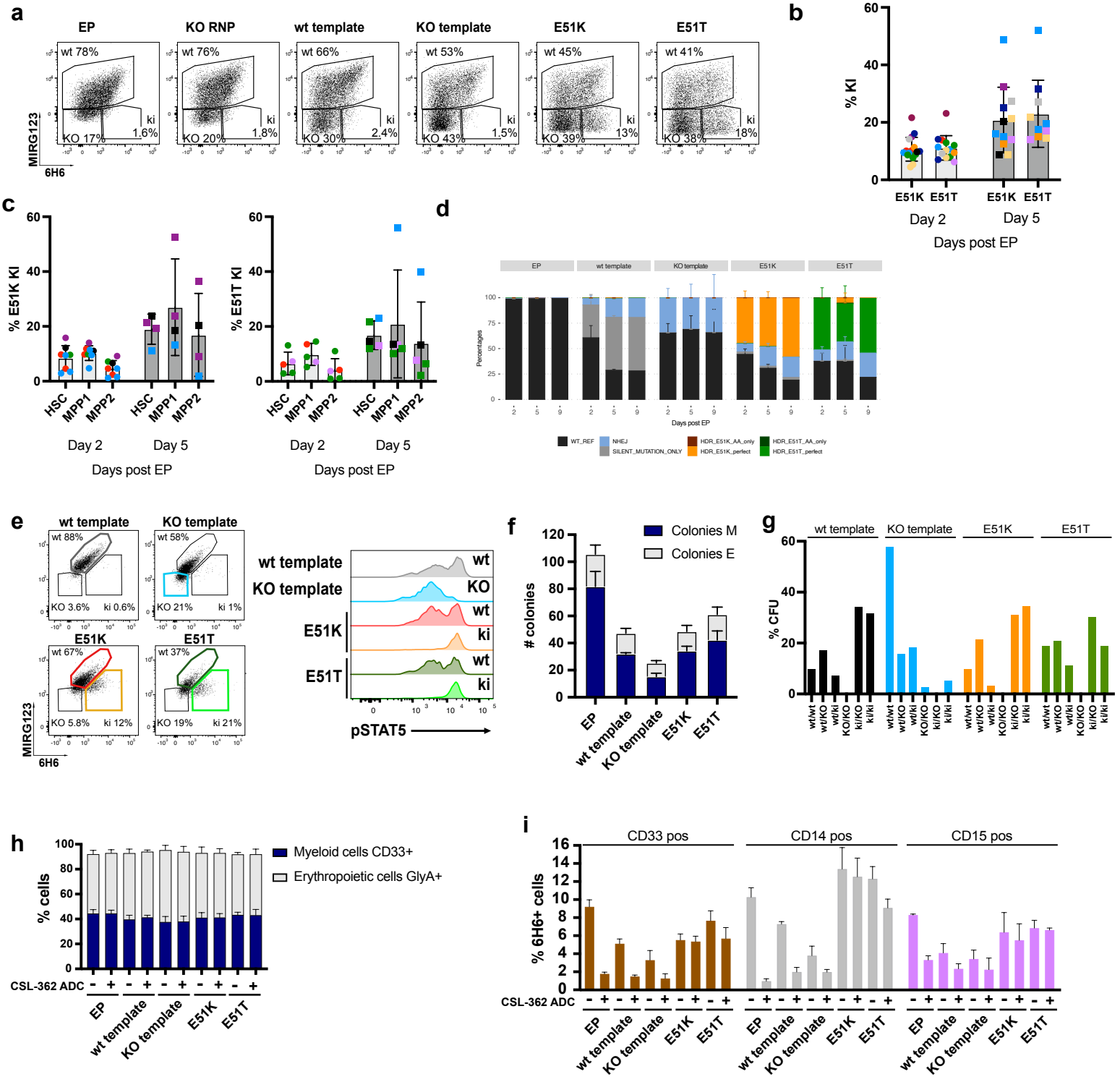
a
EP
KO RNP
wt template
KO template
E51K
E51T
wt 78%
wt 76%
wt 66%
wt 53%
wt 45%
wt 41%
ki 1.6%
ki 1.8%
ki 2.4%
ki 1.5%
ki 13%
ki 18%
KO 17%
KO 20%
KO 30%
KO 43%
KO 39%
KO 38%
MIRG123
6H6
b
% KI
E51K E51T E51K E51T
Day 2
Day 5
Days post EP
c
% E51K KI
% E51T KI
HSC MPP1 MPP2
Day 2
Day 5
Days post EP
d
Percentages
Days post EP
WT_REF
NHEJ
SILENT_MUTATION_ONLY
HDR_E51K_AA_only
HDR_E51K_perfect
HDR_E51T_AA_only
HDR_E51T_perfect
e
wt template
KO template
wt 88%
wt 58%
KO 3.6%
ki 0.6%
KO 21%
ki 1%
E51K
E51T
wt 67%
wt 37%
KO 5.8%
ki 12%
KO 19%
ki 21%
MIRG123
6H6
wt template
KO template
E51K
E51T
wt
KO
wt
ki
wt
ki
pSTAT5
f
Colonies M
Colonies E
colonies
EP
wt template
KO template
E51K
E51T
g
wt template
KO template
E51K
E51T
% CFU
wt/wt
wt/KO
wt/ki
KO/KO
ki/KO
ki/ki
h
Myeloid cells CD33+
Erythropoietic cells GlyA+
% cells
CSL-362 ADC
EP
wt template
KO template
E51K
E51T
i
CD33 pos
CD14 pos
CD15 pos
% 6H6+ cells
CSL-362 ADC
EP
wt template
KO template
E51K
E51T
j
Off-target distance
gRNA
0 1 2 3
HBB 0 0 2 44 low benchmark
CD123 0 0 1 5 OT1-6
VEGFA2 0 0 7 117 high benchmark
k
DISCOVER-Seq Off Targets
PAM
DISCO Score
Mismatches
Coordinates
GTCTTTAACACACTCGATATNGG
207 Target OnT: chrX:1345397-1345416
9 7 OT7: chr4:98393545-98393564
9 7 OT8: chr5:76852262-76852281
9 7 OT9: chr6:117017325-117017344
8 7 OT10: chr17:74873985-74874004
7 5 OT11: chr11:77447109-77447128
7 6 OT12: chr1:230302954-230302973
7 6 OT13: chr2:209774760-209774779
7 6 OT14: chr6:104499843-104499862
7 7 OT15: chr11:123716422-123716441
7 7 OT16: chr2:161232988-161233007
7 7 OT17: chr5:164782381-164782400
l
Edited
Unedited
% Indels
OnT
OT
m
unedited
CD123
CD123

Figure 5. HSPCs expressing CD123 variants E51K and E51T are functional, differentiate normally in vitro and display a good safety profile

a-m, Characterization of non-virally CRISPR/Cas9-edited human $CD34^+$ HSPCs. **a,** Representative flow cytometry plots showing binding (%) of the anti-human CD123 antibody clones 6H6 and MIRG123 to edited $CD34^+$ HSPCs five days after electroporation. EP (cells electroporated with Cas9 protein only), KO RNP (electroporation with RNP only), wt template, KO template, and CD123 E51K or E51T variants (electroporated with respective HDRT). **b,** Frequency of KI cells ($MIRG123^-6H6^+$) two and five days after electroporation. Data from 8 individual donors (each a color) performed in 6 independent experiments with 2 to 4 technical replicates. **c,** Quantification of the KI population in long-term repopulating HSCs (LT-HSC; $CD34^+CD38^-CD90^+CD45RA^-$), multipotent progenitor 1 (MPP1; $CD34^+CD38^-CD90^-CD45RA^-$) and MPP2 ($CD34^+CD38^-CD90^-CD45RA^+$). **d**, Representative Amplicon-NGS sequencing of the targeted CD123 locus at 2, 5 and 9 days post-editing of control (EP), wt template, KO template, E51K and E51T conditions. Data from 4 different experiments performed with different donors were pooled. **e,** Representative FACS plots of CD123 stained with 6H6 and MIRG123 (left) and histograms of phosphorylated STAT5 (right) upon exposure to IL-3 in non-virally edited HSPCs. Color-coding in FACS plots and histogram is identical. Data represents 4 independent experiments. **f,** In vitro differentiation of CD123-engineered HSPCs assessed by number of Colony Forming Units (erythroid: E, myeloid: M). CFU were scored using STEMVision based on morphological characteristics. **g,** Allele frequency of the CD123-engineered HSPCs in minimum of 38 colonies. **h,** Frequency of GlycophorinA $(GlyA)^+$ and $CD33^+$ non-virally edited HSPCs cultured in high cytokine medium with or without CSL-362-ADC for fourteen days. Myeloid lineage: $CD33^+$ Erythroid lineage: $GlyA^+$. Data from three experiments performed in triplicates. **i,** Frequency of $6H6^+$ CD123-positive cells in the $CD33^+$, $CD14^+$ or $CD15^+$ subsets. **j,** Computational off-target prediction. HBB and VEGFA2 as benchmarking gRNAs. On-target (OnT), Off-target (OT1-6). **k,** DISCOVER-Seq in KO RNP edited HSPCs. On-target (OnT), Off-target (OT7-17). **l,** rhAMPSeq validation of computational prediction and DISCOVER-Seq analysis. Shown are the editing rates as percentage of indels detected at the on-target (OnT) site and at the 17 off-target (OT) sites. Blue circles: Edited category comprises samples treated with gRNA for CD123 (KO RNP, KO template, E151K and E15T). Red triangles: Unedited category comprises samples not treated with gRNA for CD123 (HSC, EP). Samples were obtained from 5 different experiments and donors. **m,** CAST-Seq in unedited and KO RNP edited HSPCs. Coverage plots of the on-target site in *CD123* indicate large inversions (pink line) and deletions (orange line), respectively. Circos plot is used to illustrate chromosomal translocations.

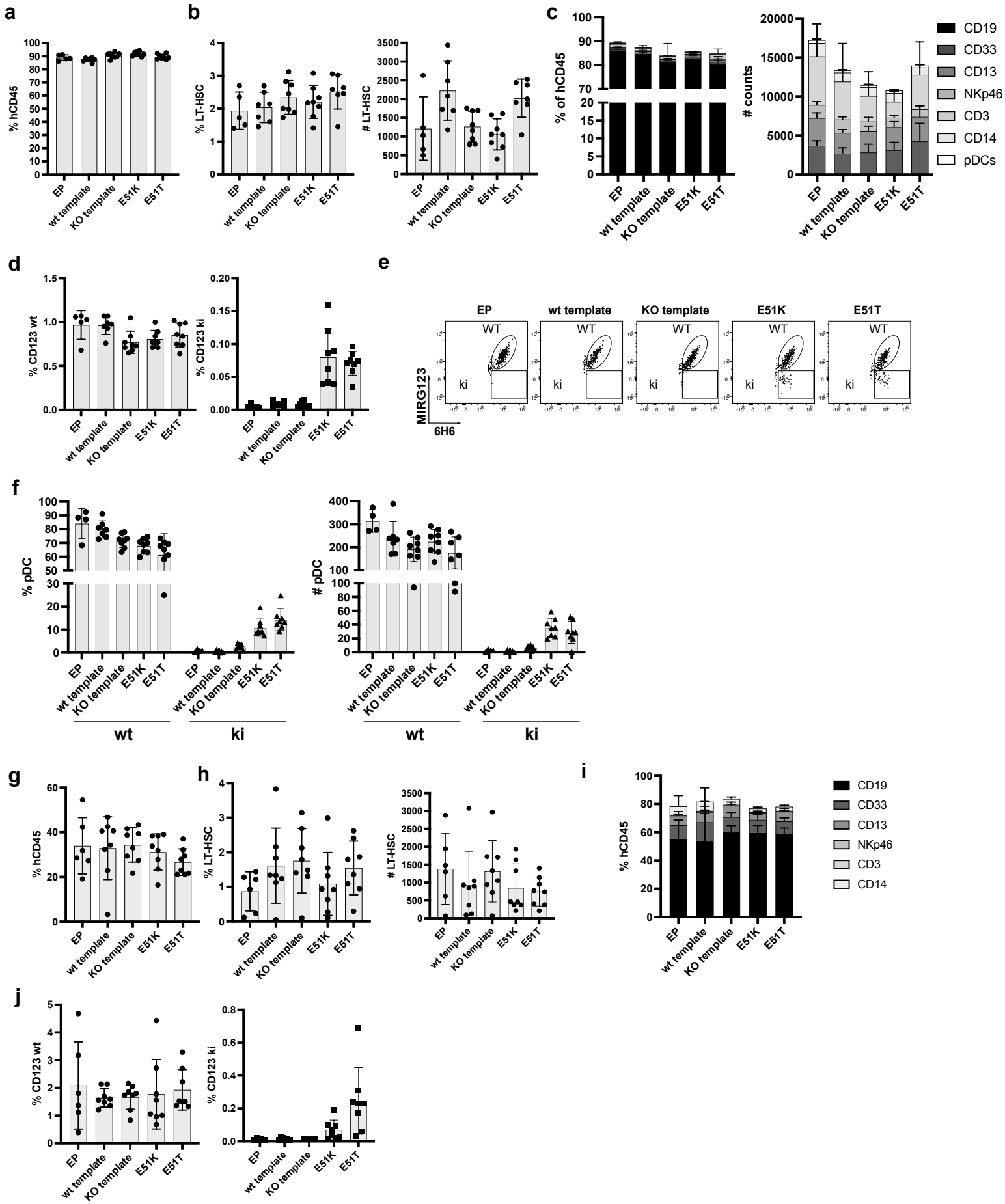
a
% hCD45
b
% LT-HSC
# LT-HSC
c
% of hCD45
# counts
CD19
CD33
CD13
NKp46
CD3
CD14
pDCs
d
% CD123 wt
% CD123 ki
e
EP
wt template
KO template
E51K
E51T
WT
ki
MIRG123
6H6
f
% pDC
# pDC
wt
ki
g
% hCD45
h
% LT-HSC
# LT-HSC
i
% hCD45
j
% CD123 wt
% CD123 ki

Fig. 6. CD123 epitope engineered HSPCs engraft, differentiate normally and possess longterm reconstitution potential in vivo

a-f, In vivo engraftment and differentiation potential of non-virally engineered HSPCs expressing E51K and E51T variants measured 16 weeks after injection in NBSGW mice. **a,** Human chimerism (% $hCD45^+$) in bone marrow. **b,** Proportion and absolute number of $CD34^+CD38^-CD90^+CD45RA^-$ HSCs in the bone marrow. **c**, Multi-lineage differentiation in spleen. Proportions and absolute numbers are shown. **d,** Proportion of wt CD123 (MIRG123+ and 6H6+) **(left)** or CD123 ki (MIRG123- and 6H6+) **(right)** gated on human CD45. **e,** Representative dot plot of pDCs stained with MIRG123 and 6H6 in spleen. Gating strategy to identify pDCs depicted in Extended data Fig.4. **f,** Proportion and absolute number of pDCs. **g-j**, Secondary transplant into NSG-SGM3 mice. **g,** Human chimerism (% $hCD45^+$) in bone marrow. **h,** Proportion and absolute number of $CD34^+CD38^-CD90^+CD45RA^-$ HSCs in the bone marrow. **i**, Multi-lineage differentiation in spleen. **I,** Proportion of wt CD123 (MIRG123+ and 6H6+) **(left)** or CD123 ki (MIRG123- and 6H6+) **(right)** gated on human CD45. **a-j,** Error bars: mean ± SD.

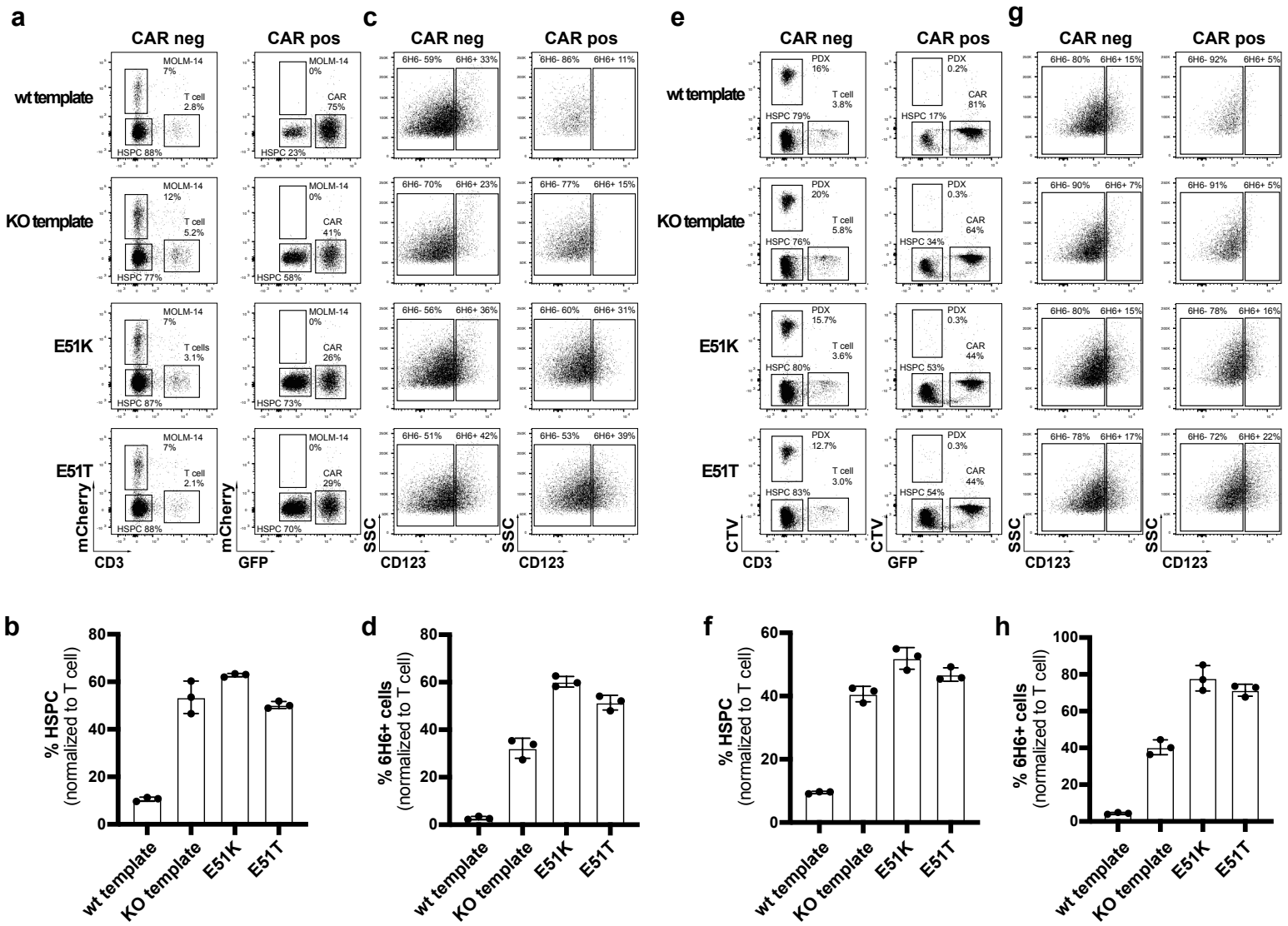

Figure 7. Engineered HSPCs enable tumor-selective CD123 immunotherapy

a-d, Non-virally edited HSPCs co-cultured with MOLM-14-mCherry (AML cells) and control T cells or 123CAR for 2 days. **a,** Representative dot plots indicating proportion (%) of $CD3^+$T cells, MOLM-14 cells and non-virally edited $CD34^+$ HSPCs on day 2 of co-culture. **b,** Quantification of **(a)** based on absolute counts. **c**, FACS plots illustrating proportion (%) of wt or ki HSPCs at the end of the co-culture based on the binding characteristics to the mAb 6H6. Only clone 6H6 was used to avoid epitope masking by the 123CAR. **d,** Quantification of **(c)** based on absolute counts. **e-h,** Non-virally edited HSPCs co-cultured with PDX (CTV labeled) and control T cells or 123CAR for 2 days. **e,** Representative dot plot indicating proportion (%) of $CD3^+$T cells, PDX cells and non-virally edited $CD34^+$ HSPCs on day 2 of co-culture. **f,** Quantification of **(e)** based on absolute counts. **g**, FACS plots illustrating proportion (%) of wt or ki HSPCs at the end of the co-culture based on the binding characteristics to the mAb 6H6. **h,** Quantification of **(g)** based on absolute counts. Data normalized to co-culture with T cells. **a-h,** Error bars: mean ± SD.